Configuration and Timing of Collision between Arabia and Eurasia in the Zagros Collision Zone, Fars, Southern Iran

Fulong Cai, Lin ding, Houqi Wang, Andrew K. Laskowski, Liyun Zhang, Bo Zhang, Ali Mohammadi, Jinxiang Li, Peiping Song, Zhenyu Li, Qinghai Zhang

Fulong Cai et al, 2021, Configuration and Timing of Collision Between Arabia and Eurasia in the Zagros Collision Zone, Fars, Southern Iran, Tectonics, 40, Citation number, 10.1029/2021TC006762. To view the published open abstract, go to https://doi.org/10.1029/2021TC006762

AGU ADVANCING EARTH AND SPACE SCIENCE

Tectonics

RESEARCH ARTICLE
10.1029/2021TC006762

Key Points:

- Neyriz ophiolite was obducted onto Arabia during Late Cretaceous-early Paleocene time
- Arabia-Eurasia intercontinental collision occurred before deposition of 25.7–21.5 Ma Razak formation
- Decreases in propagation rate of foreland basin system play an important role in the growth of high elevation orogenic plateau

Supporting Information:

Supporting Information may be found in the online version of this article.

Correspondence to:

F. Cai,
flcai@itpcas.ac.cn

Citation:

Cai, F., Ding, L., Wang, H., Laskowski, A. K., Zhang, L., Zhang, B., et al. (2021). Configuration and timing of collision between Arabia and Eurasia in the Zagros collision zone, Fars, southern Iran. *Tectonics*, *40*, e2021TC006762. https://doi.org/10.1029/2021TC006762

Received 11 MAY 2021
Accepted 5 AUG 2021

Configuration and Timing of Collision Between Arabia and Eurasia in the Zagros Collision Zone, Fars, Southern Iran

Fulong Cai[1], Lin Ding[1], Houqi Wang[1], Andrew K. Laskowski[2], Liyun Zhang[1], Bo Zhang[3], Ali Mohammadi[4], Jinxiang Li[1], Peiping Song[1], Zhenyu Li[1], and Qinghai Zhang[1]

[1]State Key Laboratory of Tibetan Plateau Earth System Science, Resources and Environment, Institute of Tibetan Plateau Research, Chinese Academy of Sciences, Beijing, China, [2]Department of Earth Sciences, Montana State University, Bozeman, MT, USA, [3]School of Earth and Space Sciences, The Key Laboratory of Orogenic Belts and Crustal Evolution, Peking University, Beijing, China, [4]Eurasia Institute of Earth Sciences, Istanbul Technical University, Istanbul, Turkey

Abstract The configuration and timing of the Arabia-Eurasia continental collision, part of the broader Alpine-Himalayan collisional system, remains controversial. We conducted sandstone petrology, detrital zircon U-Pb-Hf isotopic and trace element analysis, and Cr-spinel electron microprobe geochemical analysis of samples from Paleocene to Miocene peripheral foreland strata in interior Fars, southern Iran. These data were used to test competing models for ophiolite obduction and Arabia-Eurasia collision. In addition, we applied these data to compare the history of outward and upward growth of the Zagros and Himalayan-Tibetan segments of the Alpine-Himalayan collisional orogenic belt. The first appearance of radiolarian-rich chert conglomerate, 100–90 Ma detrital zircons with positive $\varepsilon Hf(t)$ values from +1 to +20 and midocean ridge geochemical affinity, and suprasubduction zone (SSZ) affinity Cr-spinel is in the lower and middle Sachun Formation. These data indicate that obduction occurred before deposition of the upper Maastrichtian-lower Paleocene Sachun Formation and developed in an intra-oceanic setting rather than an Arabia-Eurasia collision setting. Abundant continental-arc affinity detrital zircon with 180–160 Ma and 50–27 Ma age-probability peaks and varied $\varepsilon Hf(t)$ values are present in the upper Oligocene-lower Miocene Razak and Agha Jari formations, indicating sedimentary overlap with Eurasia. SSZ-affinity Cr-spinel in all samples indicates that ophiolitic rocks were a continual source of detritus in the foreland basin since Paleocene. The depositional age of the basal Razak Formation is between 25.7 and 21.5 Ma. Therefore, we interpret that collision between Arabia and Eurasia must have been initiated before deposition of the Razak Formation.

1. Introduction

Closure of the Neo-Tethyan Ocean and resultant intercontinental collisions created the high topography of the Alps in southern Europe, the Iran plateau in the Middle East, and the Himalaya-Tibetan Plateau in southeast Asia. These belts are commonly divided into Alpine, Zagros, and Himalayan orogens along strike (Hatzfeld & Molnar, 2010; Yin & Harrison, 2000). Each segment can be considered similar in tectonic settings but each is characterized by distinct topographic characteristics, timing of collision onset, convergence magnitudes, and tectonic histories (Hatzfeld & Molnar, 2010). Considered together, they are a vast natural laboratory for understanding the process of inter-continental collision and responses to regional variation in boundary conditions. A critical step in analyzing this system is to determine the timing of collision and precollisional margin configuration for each segment. Onset timing in the Zagros collisional belt is critically important for relating convergence to crustal shortening (Pirouz et al., 2017), understanding expansion and uplift of Zagros-Iranian plateau and associated Cenozoic climate change (Allen & Armstrong, 2008; Mouthereau et al., 2012), developing regional dynamic models, and understanding the opening of the Red Sea and Aegean Sea (Hatzfeld & Molnar, 2010; McQuarrie & van Hinsbergen, 2013). Despite this importance, the geometry and timing of the initial Arabia-Eurasia continental collision are not well known. One hypothesis is that Arabia and Eurasia collided directly without any preceding ophiolite obduction and/or intraoceanic arc accretion (Alavi, 1994, 2004; Berberian & King, 1981). An alternative hypothesis involves

obduction of Neo-Tethyan ophiolites onto Arabia during Late Cretaceous time followed by Arabia-Eurasia collision onset tens of millions of years later, during latest Eocene to Oligocene time (Agard, et al., 2011; Allen & Armstrong, 2008; Ballato et al., 2011; Barber et al., 2018; Fakhari et al., 2008; Horton et al., 2008; Koshnaw et al., 2019; McQuarrie & van Hinsbergen, 2013; Mouthereau et al., 2012; Pirouz et al., 2017; Saura et al., 2015) or Miocene time (Khadivi et al., 2010, 2012; Okay et al., 2010; Zhang et al., 2017). Though contradictory, these hypotheses might be reconciled by considering variations in the setting and approach of previous studies.

The proposed timing of the Arabia-Eurasia collision strongly correlates with the location and tectonic setting of previously studied areas. For instance, studies focused on the Zagros peripheral foreland basin on the lower plate determined Oligocene-Miocene collision age (e.g., Homke et al., 2010; Mouthereau et al., 2007; Pirouz et al., 2017), whereas those focused on the Alborz mountain and central Iran regions on the upper plate determined late Eocene-early Oligocene collision age (e.g., Ballato et al., 2011; Horton et al., 2008). An additional complicating factor is the type of evidence that was used to determine the timing of collision onset or the minimum age of collision. Previous studies invoked direct evidence such as the provenance of synorogenic foreland basin sediments (Koshnaw et al., 2019), forebulge development timing (Pirouz et al., 2017), and plate tectonic reconstructions (McQuarrie & van Hinsbergen, 2013) and/or indirect evidence such as the timing of rock deformation (Mouthereau et al., 2012), the timing of the transition from oceanic to continental subduction geochemical affinities (Chiu et al., 2013), and the timing of paleoclimatic changes (Allen & Armstrong, 2008). In this study, we attempt to reconcile the various and sometimes contradictory datasets by applying direct collision onset dating techniques to synorogenic basins proximal to the collision zone between Arabia and Eurasia.

Peripheral foreland basins develop adjacent to zones of folding and thrusting related to intercontinental collision. Thus, the composition and sources of the strata in these basins reveal the timing of exposure of distinct rock units with characteristic ages or geochemical affinities. Detrital zircon geochronology of peripheral foreland basin strata has been used to determine timing and configuration of intercontinental collision in adjacent segments of the Alpine-Himalayan belt (e.g., DeCelles et al., 2014; Ding et al., 2016). Furthermore, the comparison of peripheral foreland basin migration in both the Zagros and Himalayas can also provide implications of orogenic expansion horizontally and vertically. In this study, we apply sedimentary petrology techniques including determination of Cr-spinel compositions along with detrital zircon U-Pb-Hf isotopic and paired geochemical analysis to the Upper Cretaceous to Miocene peripheral foreland basin of the interior Fars peripheral foreland basin in southern Iran. These data provide a robust record of the timing of consumption of the Neo-Tethyan ocean in the Zagros belt, leading to intercontinental collision and suturing of Arabia and Eurasia. In addition, we discuss these results in the context of studies from other segments of the Alpine-Himalayan system to investigate how and when the orogen expanded.

2. Tectonic Setting

In contrast to the Alps and Himalayas with higher elevations and thicker crust, the Zagros is in a relatively early stage of collision characterized by lower elevations and thinner crust (Hatzfeld & Molnar, 2010). The Zagros collision zone comprises the NW-trending, subparallel Cenozoic Urumieh-Dokhtar magmatic arc (UDMA), Mesozoic Sanandaj-Sirjan magmatic zone (SSMZ), and the Zagros fold-thrust belt from north to south (Berberian & King, 1981; Hassanzadeh & Wernicke, 2016). The Eurasian-affinity UDMA and SSMZ are separated from the Zagros fold-thrust belt on the Arabian plate by the Main Zagros Reverse Fault (MZRF; sometimes termed the Main Zagros Thrust, Figure 1). Our study area is in the interior Fars region adjacent to the Zagros suture zone (Figures 1 and 2).

The UDMA is exposed between the Sistan zone to the southeast and Lesser Caucasus and Alborz Mountains to the northwest. It consists of voluminous calc-alkaline volcanic rocks and minor intrusive rocks (Figure 1). Zircon U-Pb ages constrain the igneous rocks to late Paleocene to middle Miocene age (55–25 Ma), with a temporal progression from mainly continental arc-type rocks to 20–16 Ma adakitic rocks with mainly of positive $\varepsilon Hf(t)$ values (Figure 8, Alavi, 1994; Chiu et al., 2013, 2017; Verdel et al., 2011). Minor middle Jurassic granitoids are also exposed in the central UDMA (Chiu et al., 2017). Protracted Paleogene flare-ups in the UDMA can be attributed to extensional tectonism related to slab retreat or slab rollback

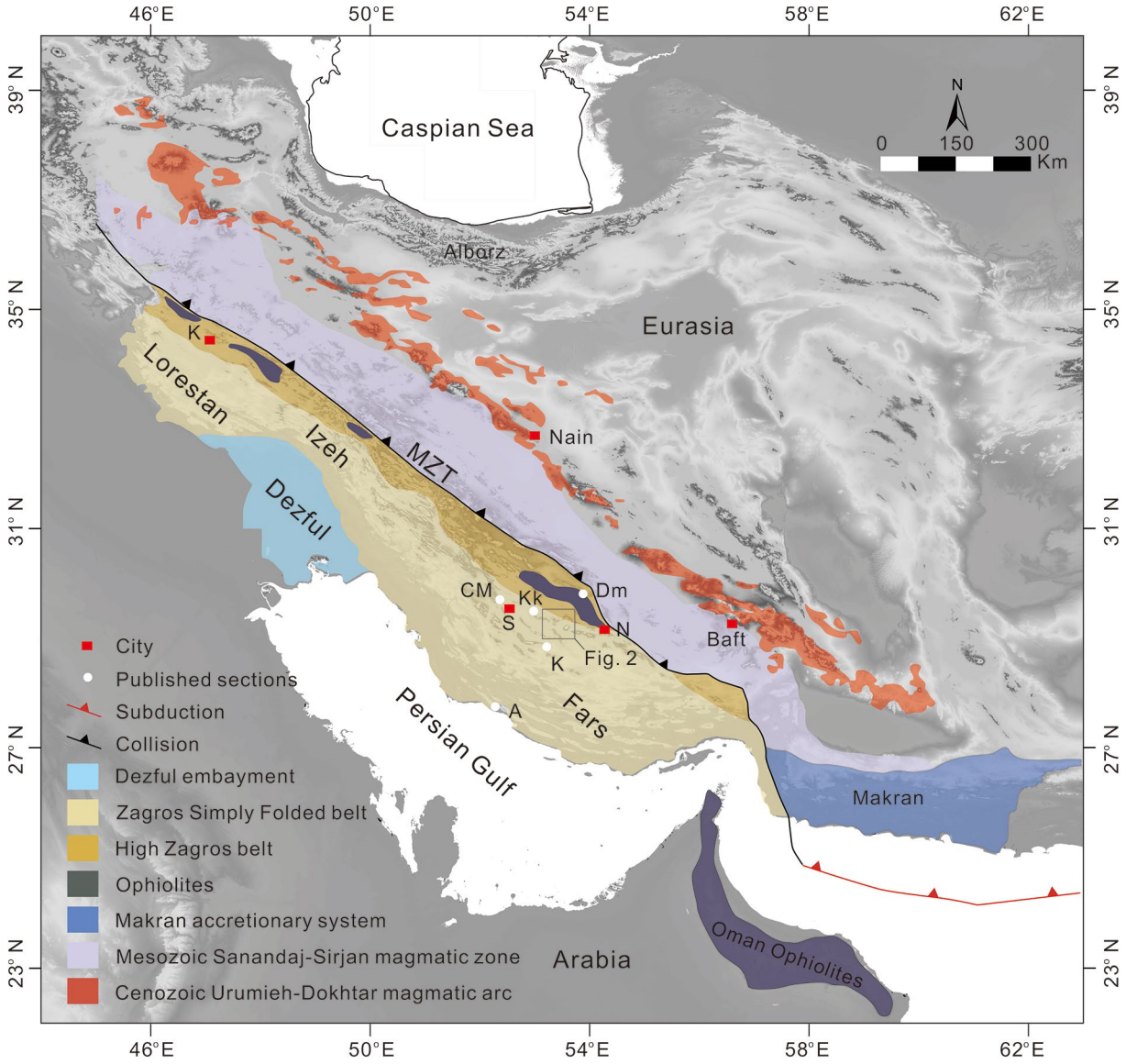

Figure 1. Regional geological map of Iran and surrounding areas superimposed on an SRTM-based digital elevation model (DEM). Geological units are modified after Pirouz et al. (2017). MZT: Main Zagros Thrust, K: Kermanshah, N: Neyriz, S: Shiraz, CM: Chahar-Makan (Khavidi et al., 2010, 2012), A: Asaluyeh (Pirouz et al., 2016), Dm: Dehmoord (Pirouz et al., 2017), K: Kaftar (Pirouz et al., 2016), Kk: Kaharak (Pirouz et al., 2016).

following the Cretaceous flat-slab subduction of Neo-Tethyan oceanic lithosphere underneath Eurasia (Verdel et al., 2011). Extensive Paleogene volcanism also occurred across the northwest, central, and eastern parts of Iran (Berberian & King, 1981). Older extensional structures were overprinted by broad retroarc folding and thrusting during Oligocene and Miocene time (Morley et al., 2009).

The SSMZ is located along the southernmost margin of the Iran microplate, representing an Andean-type continental margin that was established in Early Jurassic time (Agard et al., 2011; Chiu et al., 2013; Hassanzadeh & Wernicke, 2016; Verdel et al., 2011). Its boundary with the UDMA is the ~99–102.8 Ma Nain-Baft ophiolite belt and the 77.5–82.7 Ma volcanic-plutonic complex in the east (Hosseini et al., 2017; Shafaii Moghadam et al., 2013). The boundary between the SSMZ and UDMA is now well known in the central and western parts of Iran (Figure 1). The SSMZ consists mainly of Permian to Jurassic metamorphic and intrusive igneous rocks sometimes associated with localized pre-Cambrian basement outcrops (Hassanzadeh & Wernicke, 2016). Igneous rocks in the SSMZ include Early Jurassic calc-alkaline intrusive and extrusive igneous rocks that were generated by northward subduction of Neo-Tethyan oceanic lithosphere

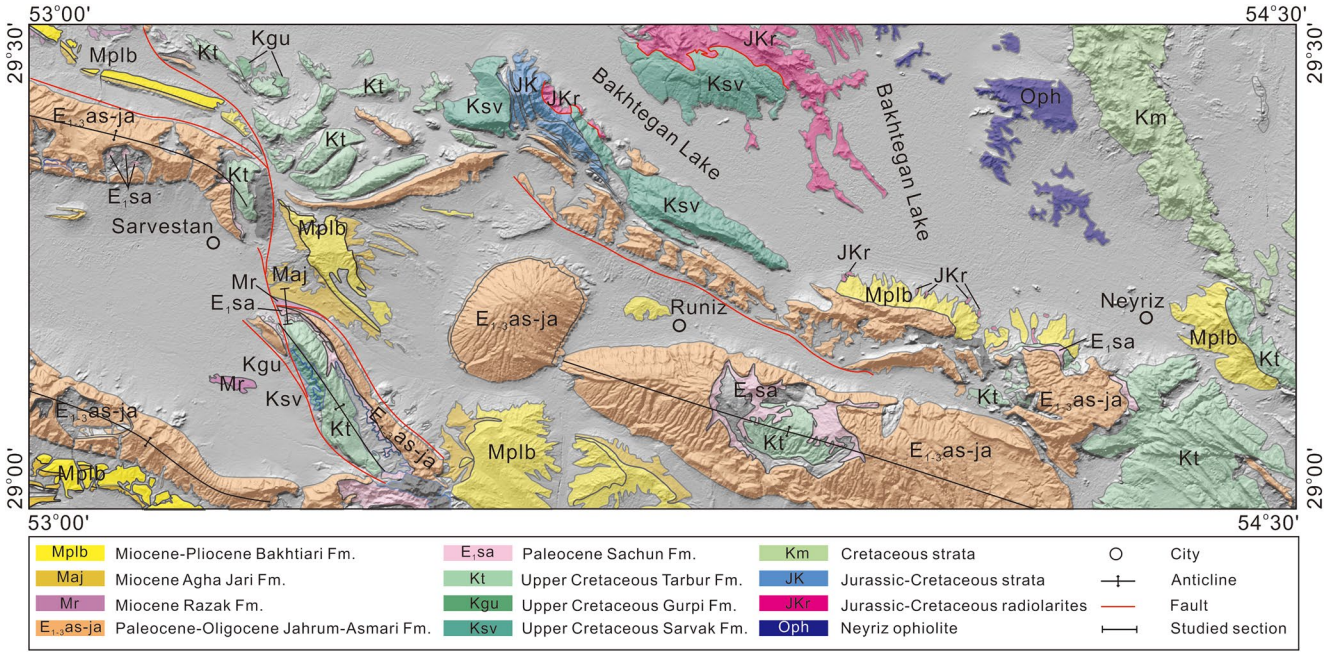

Figure 2. Detailed geological map of Sarvestan-Neyriz in the Fars region. Bedrock is modified after the 1:1,000,000 geologic map of Iran and 1:2,500,000 geological map of Neyriz and Monsef et al. (2018). Base Global Multiresolution Topography map is from http://www.geomapapp.org and Ryan et al. (2009).

(Chiu et al., 2013; Hassanzadeh & Wernicke, 2016; Zhang et al., 2018). Zircon U-Pb crystallization ages from these rocks are dominantly ~165 Ma, corresponding with varied zircon εHf(t) values from −5 to +5. In the western part of the SSMZ, εHf(*t*) values are more positive, ranging from +5 to +15 (Chiu et al., 2013; Hassanzadeh & Wernicke, 2016; Zhang et al., 2018). Carboniferous to early Permian (360–280 Ma) A-type granites associated with the opening of the Neo-Tethys ocean are exposed in the central and northwest SSMZ (Alirezaei & Hassanzadeh, 2012; Azizi et al., 2017; Honarmand et al., 2017). Minor Cretaceous leucogranites and diorite are also exposed in the central and northwest SSMZ (Shakerardakani et al., 2020). Detrital zircons from sedimentary rocks in the SSMZ predominantly produce Paleozoic-Mesozoic U-Pb ages (Hassanzadeh & Wernicke, 2016). The SSMZ experienced high-pressure metamorphism based on the presence of Early Jurassic eclogites (Davoudian et al., 2016). The overlying strata include undeformed Cretaceous limestone and Cenozoic marine and nonmarine sedimentary rocks (Hassanzadeh & Wernicke, 2016).

Remnants of Neo-Tethyan oceanic crust mark the Arabia-Eurasia suture zone to the south. Ophiolitic rocks of the Zagros suture zone (also known as "crush zone") are only exposed in the Neyriz and Kermanshah areas along the Main Zagros Thrust (Figure 1, Stocklin, 1968). In Neyriz, suture-zone rocks are composed of several thrust imbricates that include peridotite, gabbro, plagiogranite, diabase, pillow lava, Late Triassic to Late Cretaceous radiolarian chert and limestone, and tectonic mélange (Babaie et al., 2006; Lanphere & Pamic, 1983; Robin et al., 2010; Zadeh et al., 2020). The radiolarian chert was thrust over the Turnian-Campanian Sarvak Formation of the Arabian continental passive margin sequence and is unconformably overlain by the Maastrichtian Tarbur Formation (Figures 2 and 3, Hallam, 1976; Alavi, 2004; Babaie et al., 2006; Habibi & Ruban, 2018). Zircon U-Pb ages of diabase and plagiogranite indicate that the ophiolites formed between 100 and 93 Ma and are characterized by positive εHf(*t*) values ranging from +10 to +20 (Monsef et al., 2018; Shafaii Moghadam et al., 2017; ~ and reference therein). These data are similar to paired zircon U-Pb and Hf data from ophiolites in Oman and Cyprus (Warren et al., 2005). Recent work indicates that the Neyriz ophiolite experienced a geochemical evolution from midocean ridge to subduction-related affinities (Monsef et al., 2018 and references therein). In the Kermanshah area, the Zagros suture zone consists of Bisotun limestones, Jurassic-Cretaceous radiolarian chert-rich nappes, Harsin peridotites and gabbros, and basaltic lava flow deposits (Ao et al., 2016; Whitechurch et al., 2013). Zircon U-Pb ages and K-Ar ages of diabase and plagiogranite indicate that the ophiolitic rocks formed at ~36 Ma and 79–86 Ma with positive

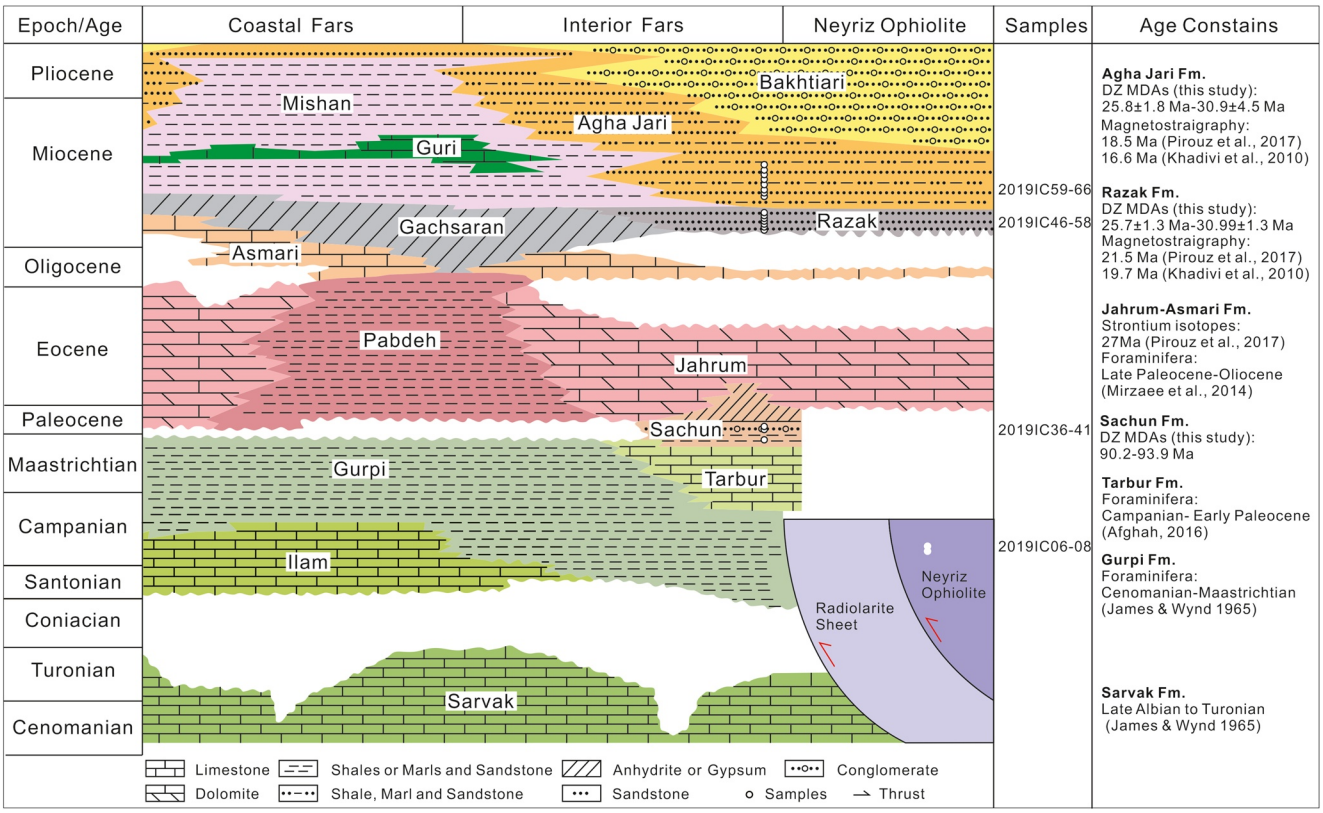

Figure 3. Stratigraphic column of peripheral foreland basin and Arabian passive continental strata in Interior and Coastal Fars and Neyriz ophiolite zone. Oligocene-Pliocene strata are modified after Pirouz (2018). Cenomanian-Eocene strata are modified after James & Wynd, 1965. Strata within the Neyriz ophiolite zone are modified based on the 1:2,500,000 geological map of Neyriz. DZ, Detrital zircon; MDAs, maximum depositional ages.

εHf(t) values ranging from +3 to +16, reflecting complex tectonic setting from continental rifting to intra-oceanic fore-arc extension and arc system (Ao et al., 2016, 2020; Delaloye & Desmons, 1980).

The Zagros Fold-Thrust Belt can be divided into several physiographic zones, including the High Zagros (or Imbricate belt), the Zagros Simply Folded Belt, and the Mesopotamian-Persian Gulf basin from northeast to southwest (Figure 1, Berberian & King, 1981). The High Zagros is composed of several imbricated and folded tectonic slices in which the oldest foreland basin strata are exposed (Mouthereau et al., 2012; Pirouz et al., 2017). Along strike, the Zagros Simply Folded Belt is separated into Lorestan, Dezfull embayment, Izeh zone, and Fars arc based on the variations in structure, deformation, and stratigraphy (Figure 1, Falcon, 1974; Sherkati & Letouzey, 2004; Stocklin, 1968). Both the Zagros Simply Folded Belt and the Mesopotamian-Persian Gulf basin are relatively less deformed than the High Zagros and consist of 12–14 km thick pre-Cenozoic Arabian passive continental margin strata and Cenozoic marine and nonmarine foreland strata. Considered together, these rocks evidence southward migration of the foredeep depozone during progressive development of the Zagros Fold-Thrust Belt (Falcon, 1974; James & Wynd, 1965; Pirouz et al., 2017, Figure 3).

3. Stratigraphy

Propagation of the flexural Zagros foreland basin system resulted in a complex stratigraphic record with significant variations in facies and thickness along and across the Zagros (Alavi, 2004). In Fars, chronostratigraphic studies indicate that the Cretaceous-Pleistocene strata are diachronous, migrating southwestward through time from interior Fars to coastal Fars (Figure 3, Najafi et al., 2020; Pirouz, 2018). The Sarvestan section in interior Fars is adjacent to the High Zagros portion of peripheral foreland basin stratigraphy (Figure 2). The section is >2 km thick and includes the Upper Cretaceous- Miocene Tarbur, Sachun,

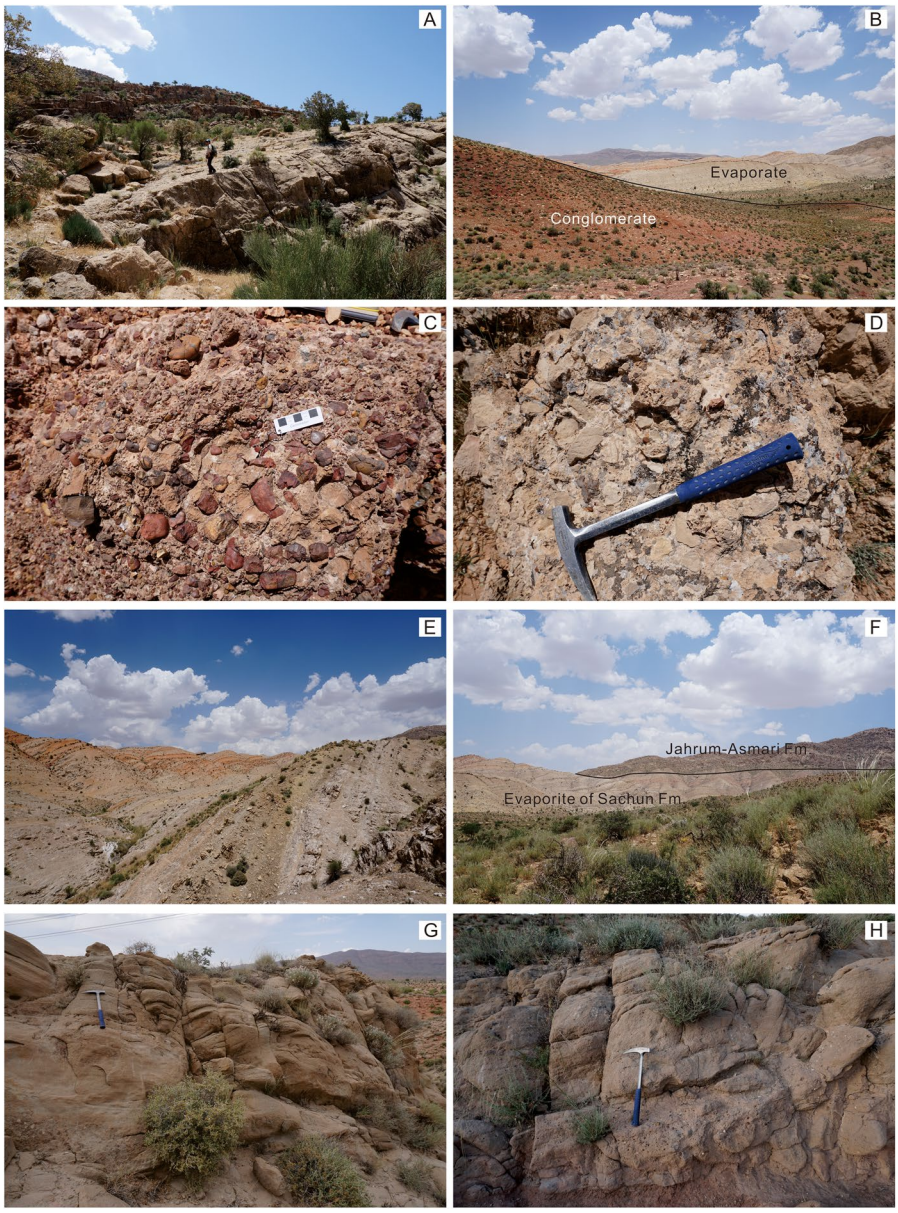

Figure 4. Photographs of Savestan section. (a) Tarbur Formation; (b) Conglomerate and Evaporite of Sachun Formation; (c) Chert-rich conglomerate of Sachun Formation; (d) Limestone-rich conglomerate of Sachun Formation; (e) Evaporite of Sachun Formation; (f) Jahrum-Asmari Formation; (g) Razak Formation; (h) Agha Jari Formation.

Jahrum-Asmari, Razak, and Agha Jari formations (Figures 2 and 3). The Tarbur Formation was deposited atop the pelagic marl and hemipelagic claystone of the Gurpi Formation and consists of light gray, thick-bedded to massive reef limestone (Figures 3 and 4a). Foraminifera indicate that the Tarbur Formation was mainly deposited during Campanian-Maastrichtian time, with local deposition continuing until Danian time (Afghah, 2016). 60 km to the east of Sarvestan, the Late Jurassic-Early Cretaceous radiolarian chert and Neyriz ophiolitic complex were thrust over the Cenomanian-Campanian Sarvak and Gurpi formations (Figures 2 and 3). The Tarbur Formation depositionally overlies these units (Figures 2 and 3, Babaie et al., 2006; Hallam, 1976). The Sachun Formation unconformably overlies the Tarbur Formation and is composed of medium-bedded, marly limestone with minor sandstone in the lower part, red conglomerate, sandstone, and mudstone in the middle part (Figures 4b–4d), and evaporites in the upper part (Figures 4b and 4e). The Sachun Formation becomes more terrigenous toward exposures of the Neyriz ophiolites (Berberian & King, 1981). Regionally, the Sachun Formation pinches out southward and is laterally equivalent

with the Amiran Formation in the Lorestan area (Alavi, 2004). These strata were deposited in a marine to nonmarine transitional environment (Alavi, 2004). Based on the ages of the underlying Tarbur Formation and overlying Jahrum-Asmari Formation, the depositional age of the Sachun Formation is roughly confined to late Maastrichtian-Paleocene time (Afghah, 2016; Alavi, 2004). The Sachun Formation conglomerates are dominated by either well-rounded radiolarian-chert or limestone clasts (Figures 4c and 4d). The Jahrum-Asmari Formation (sometimes divided into individual formations in previous mapping) is comprised of limestone, dolomite, and dolomitic limestone (Figure 4f) that was deposited during late Paleocene to early Miocene (Aquitanian) time (Amirshahkarami & Zebarjadi, 2018; Mirzaee, 2014). Limestone atop the Asmari formation was dated to ~27 Ma using Sr isotopic data from the High Zagros in the Neyriz region (Pirouz et al., 2017). The Jahrum and Asmari formations are separated by a late Eocene-early Oligocene regional unconformity (Figure 3, James & Wynd, 1965). The upper Oligocene-lower Miocene Razak Formation unconformably overlies the Jahrum-Asmari Formation and consists of conglomerate and sandstone in the lower part and multi-colored sandstone, mudstone and occasional thin-bedded evaporite in the upper part (Figure 4g). These characteristics are consistent with deposition in a restricted marine and fluvial environment (Pirouz et al., 2011). The lower conglomerates in the Razak Formation are comprised of well-rounded radiolarian-rich chert or limestone clasts, similar to the middle Sachun Formation. Magnetostratigraphy indicates that the lowermost Razak Formation was deposited at ~21.5 Ma in the High Zagros of Neyriz (Pirouz et al., 2017) and ~19.7 Ma in the Zagros Simply Folded Belt to the west of Shiraz (Khadivi et al., 2010). The Agha Jari Formation consists of thick sandstone and mudstone and minor conglomerate that was deposited in a fluvial environment (Figure 4h). The conglomeratic intervals comprise well-rounded limestone and chert fragments. Both the Razak and Agha Jari formations display cross-bedding and graded bedding. The Agha Jari Formation was deposited between 18.5 and 16.7 Ma based on magnetostratigraphy in the High Zagros, Neyriz area (Pirouz et al., 2017) and 16.6 Ma in the Zagros Simply Folded Belt to the west of Shiraz (Khadivi et al., 2010).

4. Methods and Sampling

The modal framework grain composition of each sample was determined using the Gazzi-Dickinson point counting method (Dickinson, 1985). More than three hundred grains were counted in each sample and the recalculated data are presented in Figure 6 and Table S1.

Zircon was separated from each sample using traditional crushing/grinding, density, and magnetic separation techniques. Cathodoluminescence (CL) images were obtained for each sample to guide laser ablation to avoid mixing growth zones or interpreting spurious U-Pb dates. Detrital zircon U-Pb geochronology and trace element analyses were conducted for 100–140 randomly selected grains in each sample using an Agilent 7500a ICP-MS instrument coupled with a New Wave 193 nm ArF excimer laser ablation system (New Wave Instruments, USA) at the Institute of Tibetan Plateau Research, Chinese Academy of Science, Beijing (ITPCAS). Analysis followed the methods in Cai et al. (2012). A 35-μm spot size was used during the analyses. The external standard zircons of GJ-1, Plešovice, and Qinghu yielded $^{206}Pb/^{238}U$ weighted ages of 596.6 ± 1.4 Ma (n = 198), 337.3 ± 0.68 Ma (n = 160), and 160.5 ± 2 Ma (n = 21), respectively. These are consistent with reference ages of 599.8 ± 4.5 Ma (GJ-1, Jackson et al., 2004), 337.1 ± 0.4 Ma (Plešovice, Sláma et al., 2008), and 159 ± 0.2 Ma (Qinghu, Li et al., 2013). NIST SRM 612 reference glasses were analyzed as an external standard for the trace element content. Both U-Pb ages and trace elements were calculated using GLITTER 4.0 (Macquarie University). Detrital zircon in-situ Hf isotopes were measured on the same zircon grains used for U-Pb isotopes ($^{206}Pb/^{238}U$ ages <300 Ma), using a Nu Plasma II MC-ICP-MS equipped with a NewWave 193 nm laser ablation system at ITPCAS. A 45 μm spot size was used during the analyses. Zircon standard 91,500 (0.282308 ± 6; Blichert-Toft, 2008), GJ-1 (0.282000 ± 5; Morel et al., 2008), R33 (0.282767 ± 18; Vervoor, 2010), and Qinghu (0.283002 ± 4; Li et al., 2013) were used for external correction. The measured Hf isotopic values are 0.282295 ± 48 for 91,500, 0.282010 ± 41 for GJ-1, 0.282765 ± 50 for R33, 0.283001 ± 36 for Qinghu, consistent with recommended values. Hf isotopes were calculated using Iolite V4 (University of Melbourne). Detrital zircon ages and trace elements are in Table S2; Hf isotopic data are in Table S3.

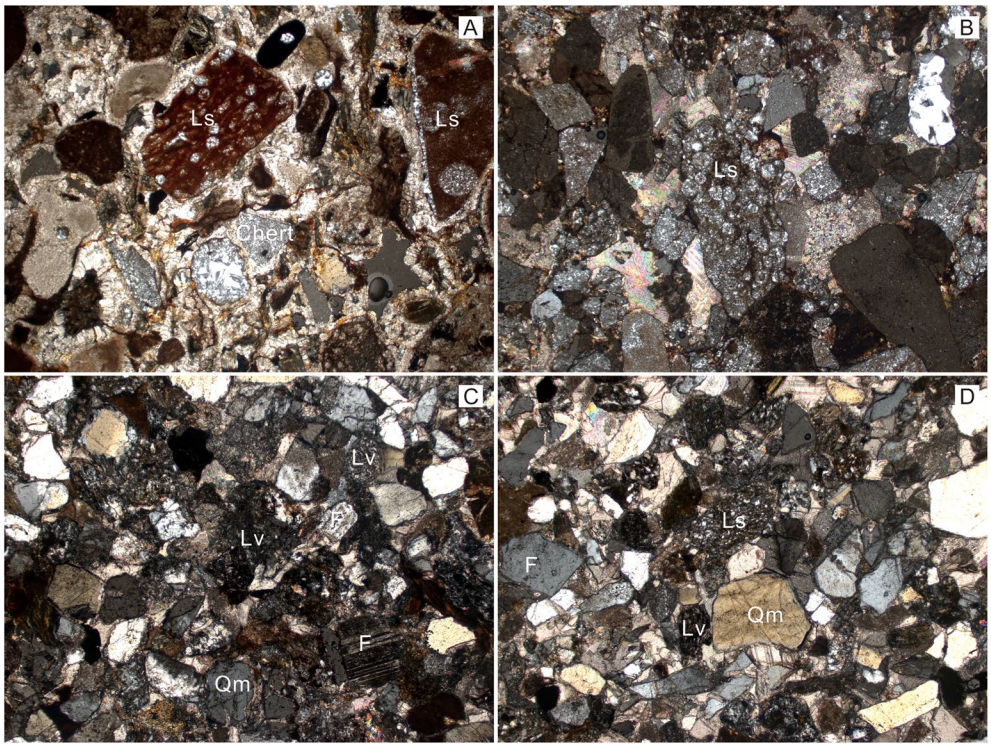

Figure 5. Photography of sandstones from the Sachun Formation, Razak Formation and Agha Jari Formation. (a) Sachun Formation, (b) Razak Formation, (c) Razak Formation, (d) Agha Jari Formation. F, feldspar; Qm, monocrystalline quartz; Lm, metamorphic lithics; Lv, volcanic lithics; Ls, sedimentary lithics.

Compositions of spinels were determined using a JXA-8230 electron microprobe Analyzer at the ITPCAS. The accelerating voltage was 21 kV, the working distance was 18 mm, the sample current was 10 nA, and the beam diameter was 1 μm. Compositions of spinels are provided in Table S4.

Maximum depositional ages (MDAs) of Paleocene-Miocene strata were determined by three methods, including the youngest single grain age (YSG), the mean age of the youngest two or more grains that overlap in age at 1σ (YC1σ(2+)), and mean age of the youngest three or more grains that overlap in age at 2σ (YC2σ(3+)) (Dickinson & Gehrels, 2009). Based on the criterion of Dickinson and Gehrels (2009), YC1σ(2+) is preferred as our maximum depositional ages (Table 1).

5. Results

5.1. Sandstone Petrography

11 medium-grained and coarse-grained sandstones (Sachun Formation, $n = 2$; Razak Formation, $n = 5$; Agha Jari Formation, $n = 4$) were sampled for sandstone petrography. Statistically, the sandstone compositions from Sachun Formation are distinguishable from that of Razak and Agha Jari formations.

Graywackes from the lower and middle Sachun Formation are poorly sorted with mostly angular to subangular clasts (Figure 5a). Sandstones from the lower limestone-dominated part consist mainly of feldspar and calcite. One sample from the middle conglomerate-dominated part is composed entirely of radiolarites-rich chert. Two additional sandstones from the middle part include polycrystalline (22%) and radiolarian-rich chert (78%). No feldspar or monocrystalline quartz was observed. These two samples plot within the recycled orogen provenance field (Figure 6). All samples contain some olivine grains. Chromite and spinel are ubiquitous heavy mineral phases.

Four poorly sorted graywackes were sampled from the Razak Formation (Figures 5b and 5c). The lower Razak Formation sample consists mainly of polycrystalline (28%) and radiolarian-rich chert (62%) with

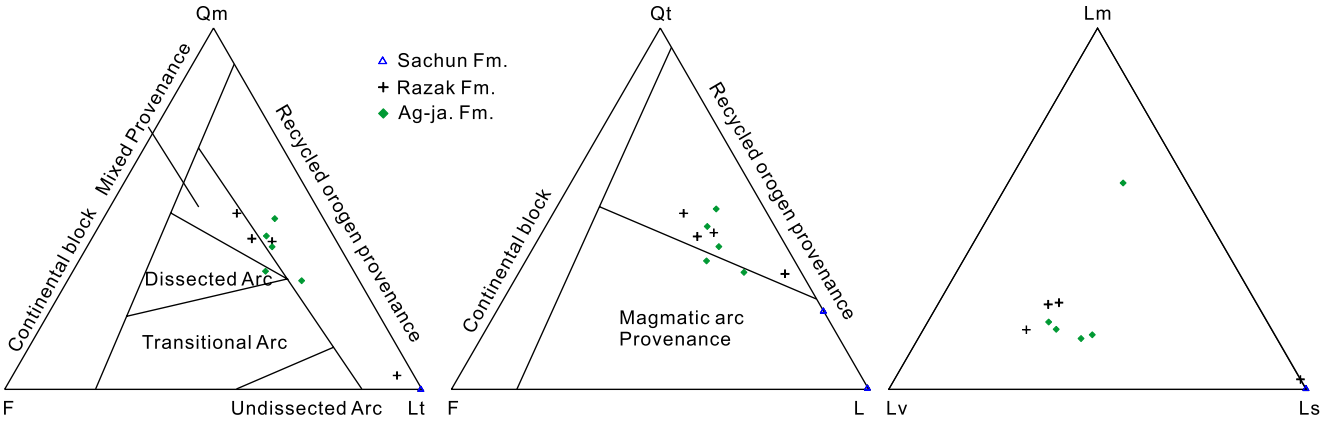

Figure 6. Ternary diagrams showing quantitative sandstone compositions from Upper Cretaceous to Eocene strata. Provenance fields after Dickinson, 1985. F, feldspar; L, lithic; Lt, total lithics; Qm, monocrystalline quartz; Qt, total quartz; Lm, metamorphic lithics; Lv, volcanic lithics; Ls, sedimentary lithics.

minor monocrystalline quartz (4%) and feldspar (4%) (Figure 5b). This is consistent with the composition of the radiolarian-chert-dominated conglomerate observed in the field. The other three samples from the upper part were poorly sorted. Quartz includes mainly monocrystalline (41%–49%) and negligible polycrystalline grains (0%–1%). Feldspar constitutes 15%–20% of the sand grains. Lithic grains (31%–41%) are composed of volcanic (18%–21%), sedimentary (8%–11%), and metamorphic (5%–10%) fragments. Sedimentary fragments are composed primarily of radiolarites-rich chert and mudstone. Metamorphic fragments are mainly of quartzite and schist. In contrast to the Sachun Formation, volcanic and metamorphic fragments first appeared in the upper Razak Formation rather than throughout the section. Rutile was also found in some metamorphic lithic fragments. Other heavy minerals include chromite and spinel. Samples from the Razak Formation plot within the recycled orogen provenance and mixed provenance fields (Figure 6).

Five graywackes were collected from the Agha Jari Formation. They are poorly sorted and consist mainly of angular to subangular grains (Figure 5d). Monocrystalline quartz (30%–47%) and feldspar (14%–21%) are major phases in all samples. Polycrystalline quartz is composed primarily of chert (no radiolarian fossils, 0%–3%), while lithic fragments are mainly volcanic (7%–28%), sedimentary (12%–17%) and metamorphic (5%–25%). The composition of metamorphic and sedimentary fragments is similar to the upper part of the Razak Formation but different than the Sachun Formation. Heavy minerals mainly include chromite and spinel. Sandstones from the Agha Jari Formation plot within the recycled orogen provenance field and along the boundary between recycled orogen provenance and magmatic arc provenance fields (Figure 6).

5.2. Detrital Zircon U-Pb Geochronology

17 samples were collected from medium- and coarse-grained sandstones in the lower and middle Sachun Formation ($n = 2$), the Razak Formation ($n = 7$), and the Agha Jari Formation ($n = 8$).

Detrital zircons from two samples (2019IC36, 2019IC39) of Sachun Formation do not display obvious oscillatory zoning, suggesting that they grew in mafic magma. The detrital zircon age spectra from the Sachun Formation samples are characterized by dominant age-probability peaks between 110 and 83 Ma (82.3%) with subordinate ages scattered between 288–201 Ma (5.7%), and 1996–510 Ma (12.0%) (Figure 7). The MDAs determined from the YC1σ(2+) method are 90.2 ± 1.1 Ma and 93.9 ± 0.66 Ma, respectively (Table 1).

Two samples (2019IC46 and 2019IC47) were collected from the lower conglomerates of the Razak Formation. 2019IC46 is characterized by abundant >400 Ma zircon (76.2%) alongside subordinate 50–27 Ma (8.0%), 192–160 Ma (5.9%), 225–308 Ma (5.9%), and 96–113 Ma (4.0%) populations. 2019IC47 is dominated by >400 Ma (74.5%) and 184-150 Ma (16.0%) zircon with subordinate 118–70 Ma (5.3%) and 294–213 Ma (4.3%) populations. The MDAs of sample 2019IC46 is 30.99 ± 1.3 Ma based on the YC1σ(2+) approach (Table 1). Samples from the upper Razak (2049IC50-58) and overlying Agah Jari formations (2049IC59-66) are very similar to each other. Prominent age-probability peaks lie in the ranges of >400 Ma (43%), 200–145 Ma (33.3%), 23–50 Ma (9.1%), and 300–200 Ma (8.7%) and alongside scattered ages between 400–300 Ma (4.7%)

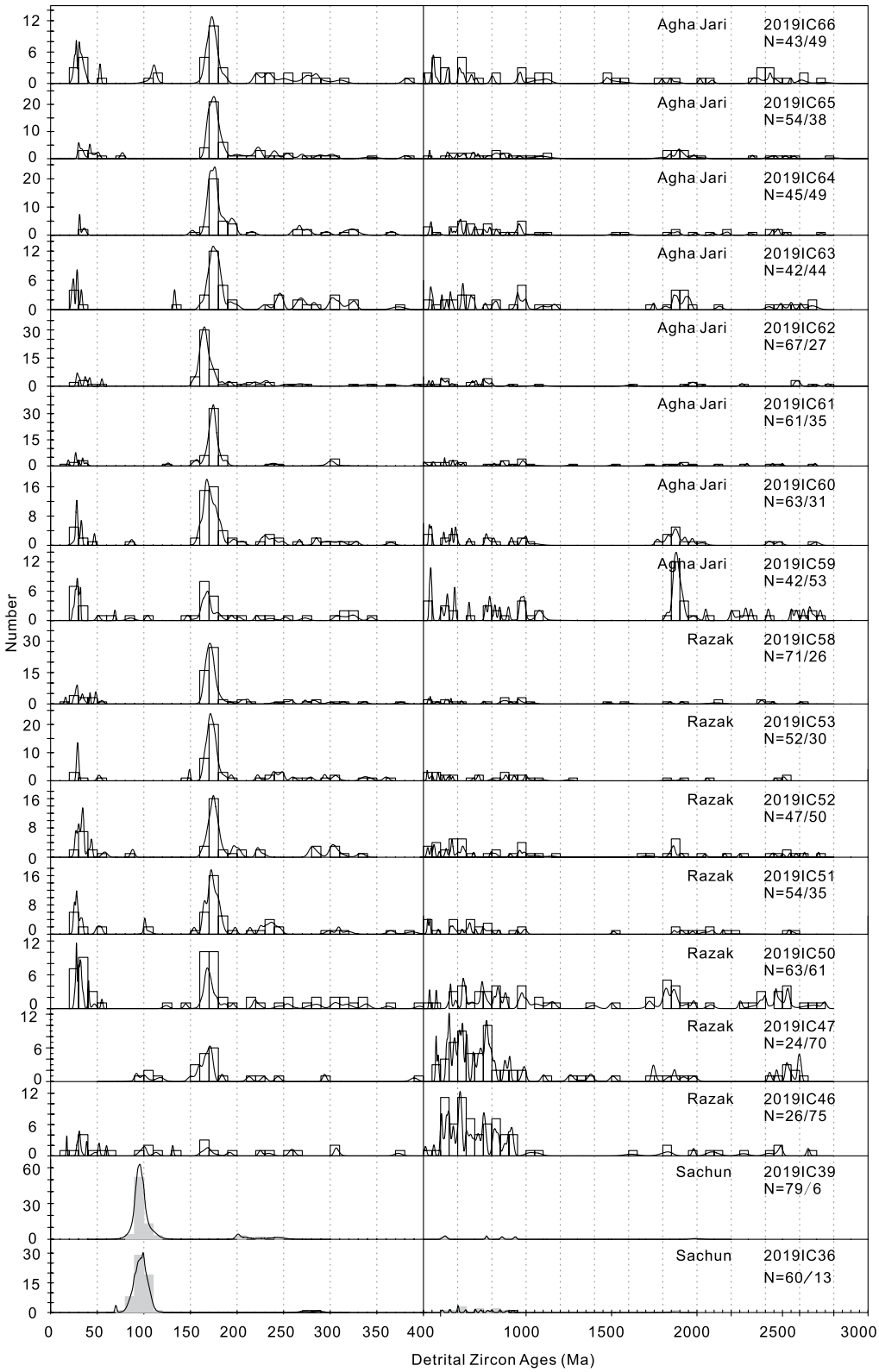

Figure 7. Detrital zircon U-Pb age probability plots of samples from the lower and middle Sachun Formation, Razak Formation, and Agha Jari Formation. Age spectra are presented with bin widths of 10 Ma for the 0–400 Ma subplot (left) and 50 Ma for the 400–3,000 Ma subplot (right).

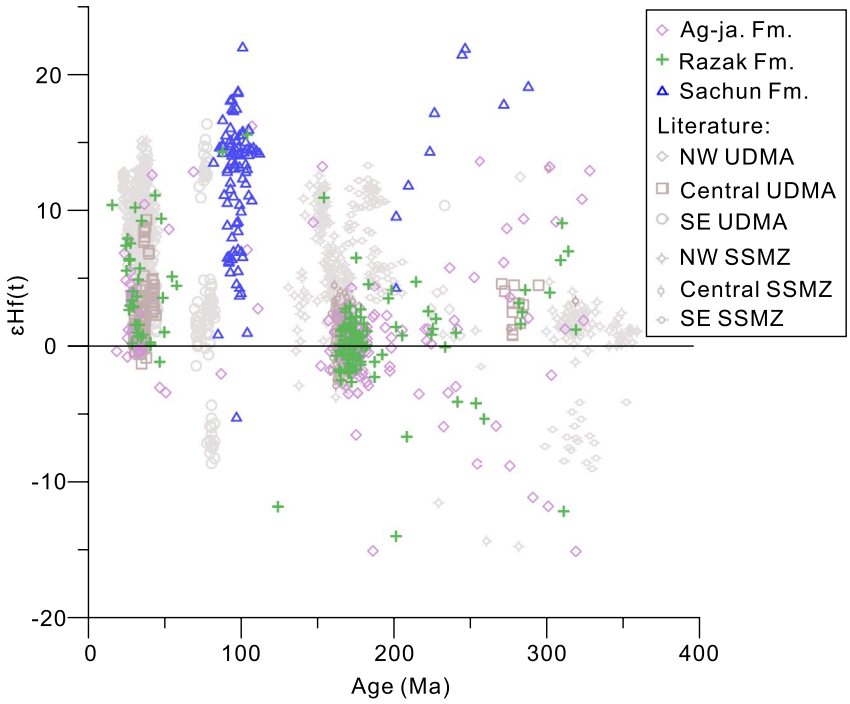

Figure 8. Detrital zircon Hf isotopes from the lower and middle Sachun Formation, Razak Formation, and Agha Jari (Ag-ja) Formation. Zircon U-Pb-Hf data of Urumieh-Dokhtar magmatic arc (UDMA) and Sanandaj-Sirjan magmatic zone (SSMZ) from literature: Chiu et al., 2017; Shafaii Moghadam et al., 2017; Zhang et al., 2018. NW: North west, SE: South east.

and 77–111 Ma (0.8%) (Figure 7). The 200–145 Ma and 50–23 Ma populations make their first appearance in the Razak and Agah Jari formations (Figure 7). The YC1σ(2+) MDAs of upper Razak formation samples are between 29.0 ± 0.93 Ma and 25.7 ± 1.3 Ma, whereas those of the AghaJari Formation are between 30.9 ± 4.5 Ma and 25.8 ± 1.8 Ma (Table 1).

Table 1
Maximum Depositional Ages of the Sachun, Razak, and Agha Jari Formations

Sample no.	Formation	*n*	YSG	YC1σ(2+)	MSWD	Cluster n	YC2σ(3+)	MSWD	Cluster n
2019IC36	Sachun	73	70 ± 1.0 Ma	90.2 ± 1.1 Ma	1.02	19	90.8 ± 1.2 Ma	1.2	22
2019IC39	Sachun	84	82 ± 11 Ma	93.9 ± 0.66 Ma	0.94	42	94.4 ± 0.71 Ma	1.3	55
2019IC46	Razak	101	17 ± 0.5 Ma	30.99 ± 1.3 Ma	0.24	3	30.10 ± 2.2 Ma	1.6	4
2019IC50	Razak	124	26 ± 1.0 Ma	27.68 ± 0.53 Ma	0.93	7	27.68 ± 0.53 Ma	0.93	7
2019IC51	Razak	89	25 ± 1.0 Ma	25.7 ± 1.3 Ma	0.14	3	27.2 ± 1.6 Ma	2.1	5
2019IC52	Razak	97	27 ± 2.0 Ma	27.5 ± 1.6 Ma	0.94	3	28.8 ± 2.4 Ma	2.1	5
2019IC53	Razak	82	28 ± 0.9 Ma	29.0 ± 0.93 Ma	0.67	4	29.0 ± 0.93 Ma	0.67	4
2019IC58	Agha Jari	97	16 ± 1 Ma	26 ± 1.4 Ma	2	2	27.8 ± 2 Ma	3.5	5
2019IC59	Agha Jari	95	24 ± 1 Ma	26.8 ± 0.98 Ma	1.08	3	27.9 ± 1.3 Ma	2.3	7
2019IC60	Agha Jari	94	26 ± 3.0 Ma	28 ± 0.99 Ma	0.21	5	28 ± 0.99 Ma	0.21	5
2019IC65	Agha Jari	93	30 ± 10 Ma	30.9 ± 4.5 Ma	1.5	3	30.9 ± 4.5 Ma	1.5	3
2019IC66	Agha Jari	92	25 ± 2 Ma	25.8 ± 1.8 Ma	0.2	2	27.1 ± 2.8 Ma	1.7	3

Note. YSG, youngest single detrital zircon age with 1-uncertainty. YC1-σ(2+), weighted mean age (±1σ-incorporating both internal analytical error and external systematic error) of the youngest cluster of two or more grain ages overlapping with the youngest age at 1-σ. YC2-σ(3+), weighted mean age (±1-σ incorporating both internal analytical error and external systematic error) of the youngest cluster of three or more grain ages overlapping with the youngest age at 2σ-(Dickinson & Gehrels, 2009).

5.3. Detrital Zircon Hf Isotopes

A subset of detrital zircon from the 110–83 Ma and 250–200 Ma U-Pb age populations in Sachun Formation samples yield positive εHf(t) values from +1 to +20 (Figure 8). In 50–30 Ma populations in the Razak and Agha Jari formation samples, most detrital zircons yield positive εHf(t) values from +1 to +12 (Figure 8). Those with U-Pb ages between 190 and 150 Ma were more variable, yielding εHf(t) values from −5 to +5 (Figure 8). Permian-Triassic detrital zircons in the Razak and Agha Jari formation samples yielded more variable εHf(t) values ranging from −15 to +15 (Figure 8).

5.4. Detrital Zircon Trace Element Geochemical Data

Trace element data obtained from detrital zircon of the Sachun Formation with Cretaceous and Permian-Triassic U-Pb ages plot in the MOR-type field on the $Log_{10}(Nb/Yb) - Log_{10}(U/Yb)$ (Figure 9) and U/Yb-Y discrimination diagrams (Figure S1). This is consistent with the compositions of the Semail, Ekecikdag, and Troodos ophiolites (Figure 9, Grimes et al., 2015). However, Tertiary, Jurassic, and Triassic-Permian age detrital zircons from the Razak and Agha Jari formations plot in the continental arc-type field on the $Log_{10}(Nb/Yb) - Log_{10}(U/Yb)$ (Figure 9) and U/Yb-Y discrimination diagrams (Figure S1) These data highlight the pronounced difference between zircon trace element compositions from the Sachun and Razak formations (Figure 9).

5.5. Chromium-Spinel Compositions

Spinel grains were separated from sandstones of the Sachun ($n = 3$), Razak ($n = 7$), and Agha Jari ($n = 8$) formations and gabbro and peridotite of the Neyriz ophiolites ($n = 2$). All Cr-spinel from Paleocene to Miocene strata have similar compositions and are indistinguishable from those of the Neyriz ophiolites (Figure 10). Out of the 436 Cr-spinels from the Sachun, Razak, and Agha Jari formations, the majority have low TiO_2 (98.8% of which ≤0.5%, 86.5% of which ≤0.2%) and Cr# between 0.22 and 0.89. Low TiO_2 (<0.2) suggests origin from mantle peridotites (Kamenetsky et al., 2001). Al_2O_3 values are in the range of 5% and 45%. All 50 Cr-spinels from the Neyriz ophiolites have low TiO_2 (≤0.21%) and Cr# between 0.38 and 0.82. Al_2O_3 values are the same as that of the detrital Cr-spinel. On the TiO_2-Al_2O_3 and TiO_2-Cr# diagrams, both the Cr-spinel from sedimentary rocks and ophiolites plot in Suprasubduction-zone (SSZ) field (Figure 10). The detrital Cr-spinels do not show clear differences between the Sachun, Razak, and Agha Jari formations.

6. Discussion

6.1. Depositional Ages of the Sachun and Razak Formations

Robust depositional ages of the Sachun and Razak formations provide independent timing constraints on the timing of ophiolite obduction and continental collision onset. The Sachun Formation lacks fossils; therefore, biostratigraphy cannot be used to provide a depositional age. Based on the underlying Maastrichtian and locally early Paleocene (Danian) Turbur Formation and overlying upper Paleocene-Oligocene Jahrum-Asmari Formation, deposition of the Sachun Formation began by late Maastrichtian-Paleocene time (Afghah, 2016; Alavi, 2004). The MDAs (Table 1, 90.2 ± 1.1 Ma and 93.9 ± 0.66 Ma) determined from the detrital zircons are older than the biostratigraphic constraints likely due to the paucity of depositional-age zircons in the source area (predominantly 90–100 Ma).

The Razak Formation unconformably overlies the Jahrum-Asmari Formation (Alavi, 2004), which was deposited during late Paleocene to early Miocene (Aquitanian) time based on benthic foraminifera in interior Fars (Mirzaee, 2014; Nadjafi et al., 2004). The weighted mean of the youngest overlapping detrital zircon ages in our Razak Formation samples is between 30.99 ± 1.3 Ma and 25.7 ± 1.3 Ma (Table 1), slightly predating the depositional ages from foraminifera. To the north, Sr isotopic data indicate that the top of the Jahrum-Asmari Formation in the High Zagros dates to ~27.6 Ma in the Dehmoord, Neyriz area (Pirouz et al., 2017). Magnetostratigraphy indicates that the lowermost Razak Formation was deposited at ~21.5 Ma in same section (Pirouz et al., 2017). The gap between 27.6-21.5 Ma was interpreted to result from a forebulge-related unconformity (Pirouz et al., 2017). To the west, the Razak Formation in the Zagros Simply Folded Belt was deposited around ~19.7 Ma based on magnetostratigraphy work in Charar Makan (Khadivi

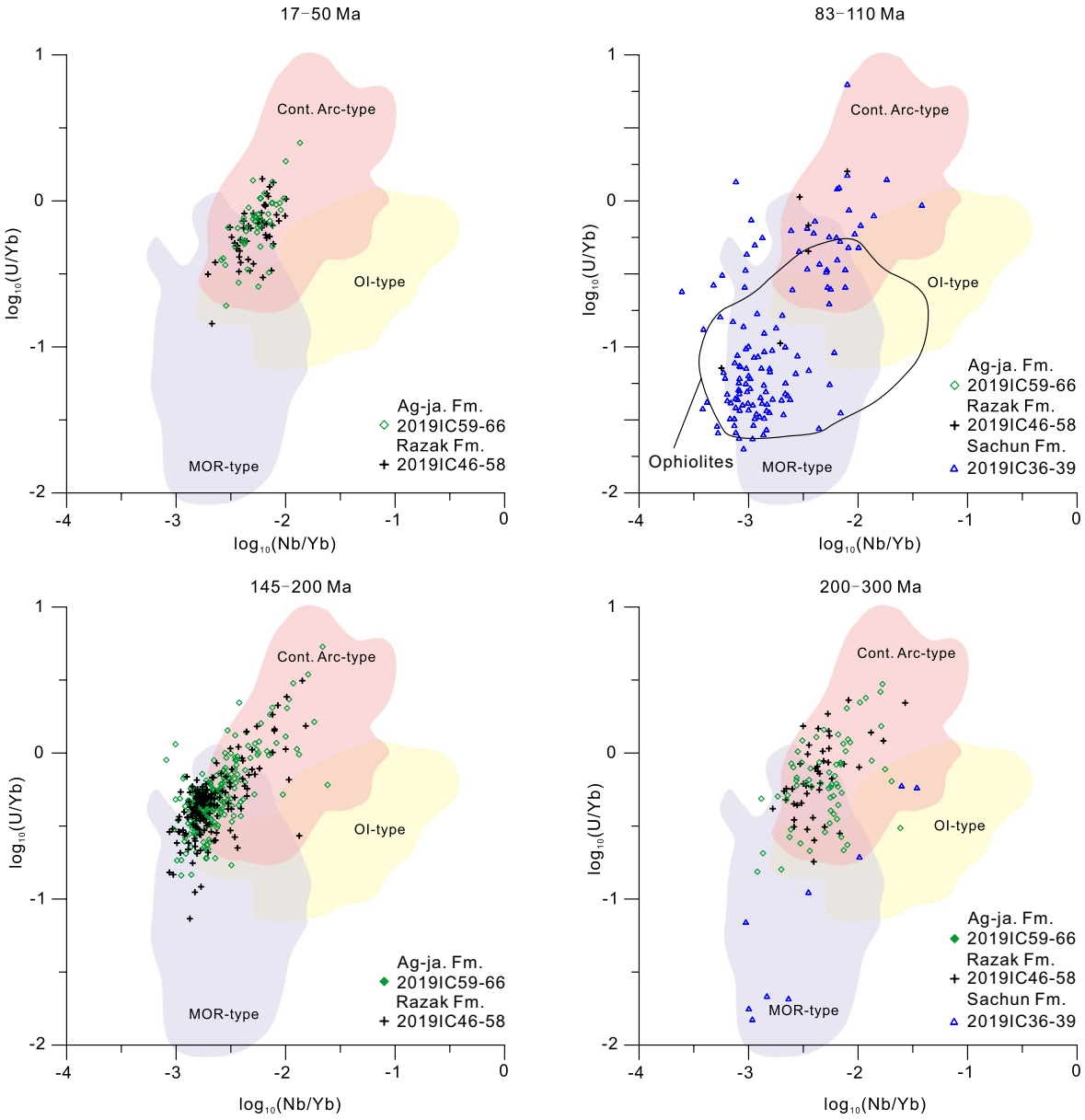

Figure 9. $Log_{10}(Nb/Yb) - Log_{10}(U/Yb)$ discrimination diagrams (Grimes et al., 2015) showing trace element data collected from detrital zircon of the Paleocene-Miocene peripheral foreland basin strata in Fars, south Iran. MOR: midocean ridge. Ophiolites field was from Grimes et al., 2015, including Semail, Ekecikdag, and Troodos.

et al., 2010) and around ~20.9 Ma in the Kaharak section (Pirouz et al., 2016). The ~19.7 Ma age from Khadivi et al. (2010) was determined at a stratigraphic position above the base of the Razak Formation. Therefore, the Razak Formation must be older than 19.7 Ma in Charar Makan (Khadivi et al., 2010). Constraints from the basal Razak Formation in Dehmoord of the High Zagros, Kaharak in the Zagros Simply Folded Belt, and Charar Makran in the Zagros Simply Folded Belt yield internally consistent early Miocene depositional ages. The similarity between depositional ages in this relatively small portion of the foreland basin system does not preclude broader scale (e.g., High Zagros to the Persian Gulf) diachronous deposition (e.g., Pirouz, 2018; Pirouz et al., 2017). Based on these data, we interpret that the basal Razak Formation was deposited between 25.7 (youngest MDAs, this study) and 21.5 Ma (magnetostratigraphic constraints in Dehmoord section, Pirouz et al., 2017) in our section.

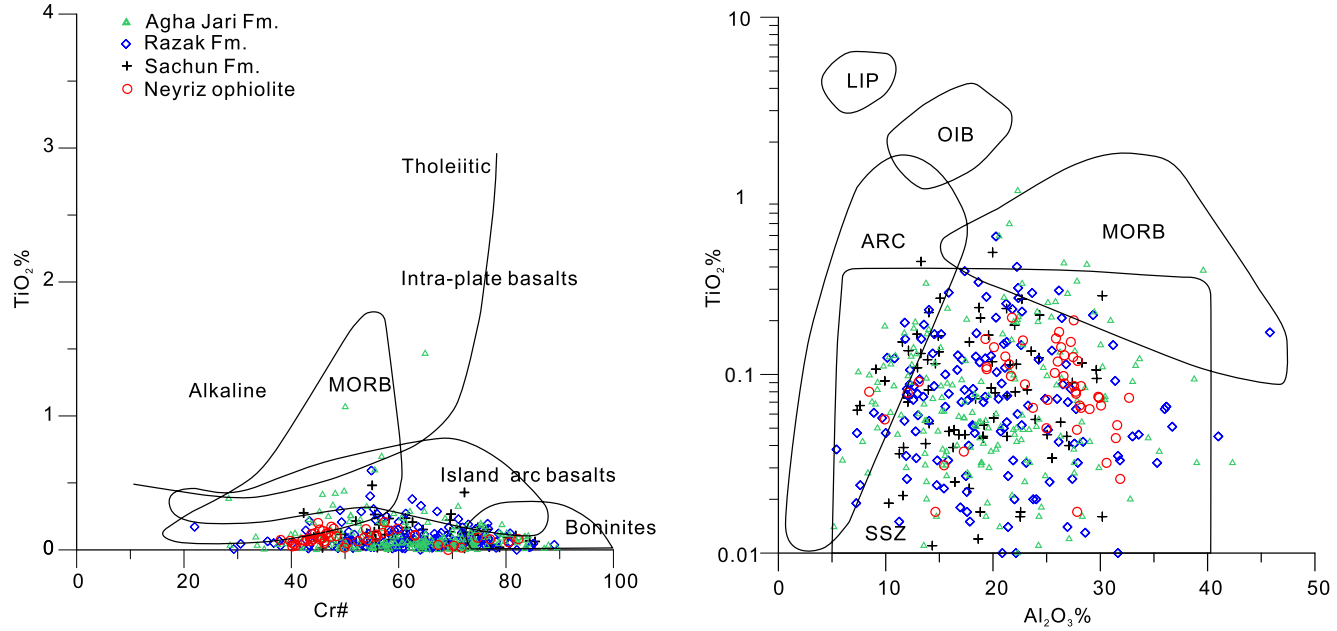

Figure 10. (a) TiO_2 versus Cr# [100*Cr/(Cr + Al)] and (b) TiO_2 versus Al_2O_3 diagrams for detrital chromium-spinels from the Sachun, Razak, and Agha Jari formations. The fields in Figure (a) are based on Kamenetsky et al. (2001). Fields in Figure (b) are based on Dick and Bullen (1984). Continental Flood Basalts (CFB), Ocean Island Basalts (OIB), Midocean Ridge Basalts (MORB), suprasubduction zone (SSZ).

6.2. Provenance Analysis of Paleocene-Lower Miocene Foreland Strata

The provenance of Paleocene-lower Miocene strata is interpreted based on sandstone petrography, population distributions of detrital zircon U-Pb ages, paired Hf isotopes and trace element, and Cr-spinel compositions.

At the base of the section, the Sachun Formation conglomerates and sandstones are composed mainly of red radiolarian-rich chert and limestone, while the sandstone samples are dominated by 100–90 Ma detrital zircon with very positive εHf(*t*) values and Neriyz ophiolitic-affinity Cr-spinels (Figures 7, 8 and 10). The Iran microplate, part of Eurasia, lacks these ages except for some xenocrystic zircon cores in the granitic rocks of the SSMZ in NW Iran (Mazhari et al., 2011). Further northeast, the inner Nain belt between the SSMZ and UDMA exposes Early Cretaceous (100–104 Ma) ophiolitic rocks (Shafaii Moghadam et al., 2013) that are slightly older than the 100–90 Ma populations of the Sachun Formation. In addition, Jurassic detrital zircon characteristics of the SSMZ are missing in the Sachun samples, indicating that the Nain belt was not in the source area. Late Cretaceous and Permian-Triassic detrital zircon in the Sachun Formation samples both have positive εHf(t) values (Figure 7) and MOR affinity (Figure 8). Therefore, it is likely that they were derived from oceanic crust, not the Eurasian-affinity SSMZ. This is also consistent with the interpretations of Cretaceous-Permian detrital zircons in the Amiran Formation in Lorestan to the west (Barber et al., 2019). The >400 Ma detrital zircons in these samples were most likely derived from the Arabian continent. All of these data suggest that no sediment derived from Eurasia is present in the Sachun Formation.

Upsection, the marine Jahrum-Asmari Formation is dominated by limestone and dolomite and lacks terrigenous deposits. The overlying Razak and Agha Jari formations are composed of quartz, feldspar and lithic fragments including volcanic, sedimentary, and metamorphic grains that are typical of recycled orogen provenance. This is different than the radiolarite- and ophiolite-affinity Sachun Formation. The composition of Miocene sandstones is similar to that of contemporaneous strata exposed in the same tectonic position in the Chahar-Makan area, excluding distinctly higher polycrystalline quartz content (Khadivi et al., 2012). Detrital zircon age spectra and Hf isotopic data from the Razak Formation are consistent with those of the Agha Jari Formation (Figures 7–9). Both formations are characterized by the coexistence of Jurassic and Eocene-Oligocene detrital zircon age-probability peaks with varied εHf(*t*) values, likely reflecting derivation from Eurasian sources, such as the SSMZ and/or UDMA (Figures 7–9). Cenozoic, Jurassic, and

Permian-Triassic detrital zircons in both the Razak and Agha Jari formations have continental arc affinity (Figure 9 and Figure S1) as opposed to MOR affinity in the Sachun Formation (this study) and Amiran Formation (Barber et al., 2019). These observations indicate that the Razak and Agha Jari formations were mainly sourced from the Eurasian continent, as both the Zagros suture zone and Arabian continent lack Jurassic and Eocene igneous rocks (Be'eri-Shlevin et al., 2009; Garzanti et al., 2013; Monsef et al., 2018; Shafaii Moghadam et al., 2017). In addition, the presence of SSZ-affinity Cr-spinels and chromite indicates that the Neyriz ophiolites continued to shed detritus into the Zagros peripheral foreland basin throughout this period (Figure 9).

6.3. Suturing Process and Neo-Tethyan Ocean Closure in the Zagros

When integrated with regional tectonic data, the changes in petrology, detrital zircon U-Pb-Hf isotopes and zircon trace element affinity throughout the Sarvestan section of interior Fars reveal the chronology of the Neyriz ophiolite obduction and transition from oceanic subduction to inter-continental collision in south Iran. Previous field observations from ~50 km east of our study area indicate that the radiolarian chert thrust sheets and Neyriz ophiolitic rocks were juxtaposed atop Cenomanian-upper Turonian Sarvak Formation by thrust faulting (Alavi, 2004; Babaie et al., 2006; Habibi & Ruban, 2018; Hallam, 1976). In turn, these rocks are depositionally overlain by the shallow marine Tarbur Formation (Hallam, 1976; James & Wynd, 1965). Given the presence of radiolarian chert fragments in Santonian-Maastrichtian strata of the Arabian continent (Khadivi et al., 2012), we postulate that the Neyriz ophiolitic rocks were initially obducted over the Arabia continental margin during Late Cretaceous time between deposition of the Cenomanian-upper Turonian Sarvak and Tarbur formations (Alavi, 2004; Babaie et al., 2006; Habibi & Ruban, 2018; Hallam, 1976). However, whether this obduction event represents the Late Cretaceous collision with an intraoceanic arc system or the onset of Arabia-Eurasia intercontinental collision is not constrained by these field observations.

In the Sarvestan section, the first appearance of ophiolite-affinity detritus occurs in the upper most Cretaceous to lower Paleocene Sachun Formation that was deposited atop the Arabian continental margin. The lack of Eurasian-affinity zircon in the Sachun Formation indicates that obduction predated Arabia-Eurasia continental collision onset (Figure 11, Alavi, 2004). This is consistent with paleomagnetic reconstructions that indicate Neo-Tethyan oceanic lithosphere still separated the obducted ophiolitic rocks and the southern margin of Eurasia during Late Cretaceous time (McQuarrie & van Hinsbergen, 2013). Our results are inconsistent with the scenario involving the first accretion of the Neyriz and Kermanshah ophiolites to the southern margin of Eurasia rather than the northern margin of Arabia (e.g., Zhang et al., 2017). The history of ophiolite obduction in the interior Fars region that best fits our data is similar to that of the Oman and Semail ophiolites, which were obducted onto the northern margin of Arabia (Hacker, 1994; Hansman et al., 2017; Searle & Cox, 1999; Warren et al., 2005).

The Amiran Formation in Lorestan was deposited in a diachronous fashion, ranging in age from Campanian in the proximal northeast Khorramabad region to Paleocene in the distal northeast Chenareh region (Saura et al., 2011). This temporal progression is consistent with the timing of obduction of radiolarian chert and ophiolitic thrust sheets during Late Cretaceous (Homke et al., 2010; Saura et al., 2011). However, an interesting phenomenon in the Fars area is that there was an apparent delay between Turonian-Campanian thrusting and radiolarian chert- and ophiolite-affinity deposition in the peripheral foreland basin system (Paleocene Sachun Formation). A possible explanation for this is that the Sachun Formation was a distal equivalent of the Amiran Formation in Lorestan, consistent with well-rounded boulders and sparse Sachun Formation outcrops in the Fars region. In contrast, the Amiran Formation is broadly exposed (Saura et al., 2011). Given that ~100 km of Arabian continental crust was subducted beneath the Eurasia continental margin (Pirouz et al., 2017), we interpret that the time delay between thrusting and deposition of terrigenous sandstone is due to underthrusting of the older Sachun Formation strata/or erosion during the obduction and intercontinental collision process.

Following complete consumption of Neo-Tethyan oceanic lithosphere, Arabia-Eurasia intercontinental collision initiated. During late Oligocene-early Miocene (25.7–21.5 Ma) time, Eurasian-affinity detrital zircon was first deposited in the Razak Formation, marking sedimentary overlap between Eurasia and Arabia (Figure 11). This significantly postdates ophiolite obduction recorded by the Sachun Formation. Although

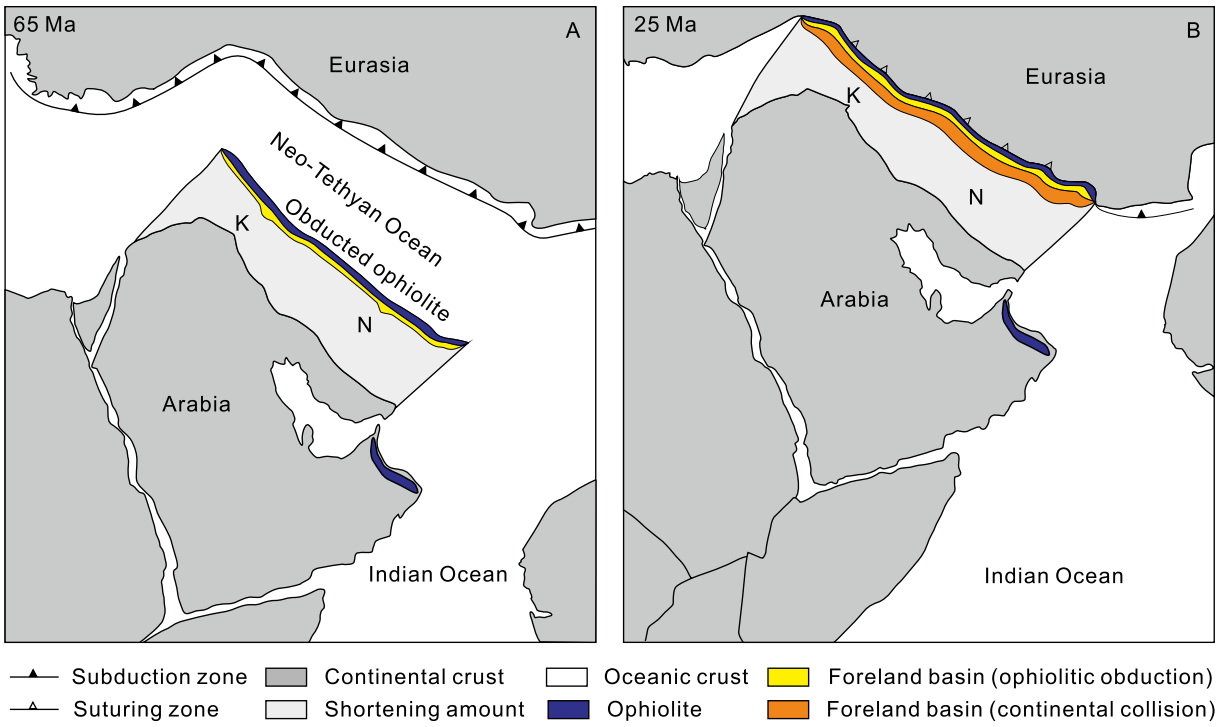

Figure 11. Simple tectonic model of Arabia-Eurasia convergence, modified after McQuarrie & van Hinsbergen, 2013. (a). the intraoceanic suture-zone rocks obducted to the Arabian continental margin since late Cretaceous and continued to the deposition of Razak Formation during latest Cretaceous-early Paleocene time. The first stage pro-foreland basin developed locally around the Neyriz and Kermanshah ophiolites. (b). the Arabia-Eurasia continental collision occurred before deposition of 25.7–21.5 Ma Razak Formation and promoted the development of the second peripheral foreland basin related to the intercontinental collision. K: Kermanshah, N: Neyriz.

the Sachun Formation is separated from the Razak Formation by the Jahrum-Asmari Formation (Figure 3), it is unlikely that collision onset occurred during deposition of Jahrum-Asmari as carbonate deposition is inconsistent with the expected increase in clastics. Our results are consistent with a 25–20 Ma cooling event affecting the SSMZ based on the detrital thermochronological results from Miocene sedimentary rocks of the Zagros foreland basin (Homke et al., 2010; Khadivi et al., 2012) and bedrocks of the SSMZ (Homke et al., 2010).

Considering the well-rounded radiolarian chert gravels in the base of the Razak Formation, facies associations, and the flexural wavelength of the foreland basin, Pirouz (2018) proposed that the Razak Formation in interior Fars represents distal deposition within the foredeep depozone. A absence of the proximal equivalent of the Razak Formation is attributed either to underthrusting beneath the Eurasian margin and/or erosion during the initial Arabia-Eurasia collision (Pirouz, 2018). Therefore, the initiation of Arabia-Eurasia intercontinental collision must have occurred before deposition of the distal Razak Formation (25.7–21.5 Ma), postdating the earliest evidence for an unconformity developed by the migrating flexural forebulge stratigraphically above the Asmari Formation (27 Ma) in the High Zagros (Pirouz et al., 2017). Along strike, the minimum age of collision is ca. 26 Ma in the Kurdistan region of Iraq (Koshnaw et al., 2019). Therefore, along-strike differences in collision age are small based on these data.

6.4. Implications for Orogenic Expansion in Zagros and Himalaya

Migration of peripheral foreland basin systems results from the propagation of peripheral fold-thrust belts during collisional orogenesis. Therefore, a comparison between the peripheral foreland basin system in the comparatively young Zagros system and the comparatively old Himalayan-Tibetan system can reveal temporal snapshots of orogenic plateaux expansion parallel to the direction of plate convergence (Hatzfeld & Molnar, 2010). This comparison has the potential to reveal processes that can be considered constants or variables relating to plateaux expansion during collisional orogenesis globally. Recent flexural modeling

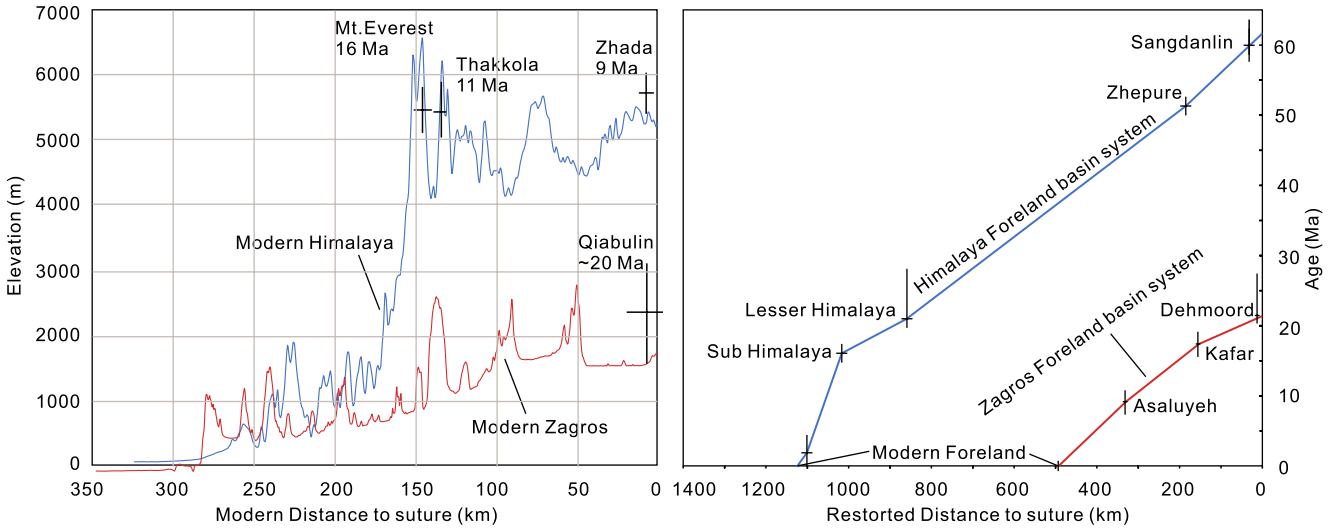

Figure 12. Comparison of peripheral foreland basin migration in Zagros and Himalaya orogen. The left panel shows elevation profiles for both the Zagros and Himalayas. The paleo-elevation data: Mt. Everest, Gébelin et al. (2013); Thakkola, Garzione et al. (2000); Zhada, Saylor et al. (2009); Qiabulin, Ding et al. (2017). In the right panel, the Himalaya foreland basin system and restored shortening are from DeCelles et al. (2014). The Zagros foreland basin system and restored shortening are from Pirouz et al. (2017).

and studies of peripheral foreland basin migration for both the Zagros (Pirouz et al., 2017) and Himalayan-Tibetan (DeCelles et al., 2014) orogenic systems enable this comparison (Figure 12).

In the Zagros, Cenozoic peripheral foreland basin deposits associated with intercontinental collision first developed in interior Fars between 25.7 and 21.5 Ma (this study; Pirouz et al., 2017), in Kaftar between 25.5 Ma and 18 Ma (Pirouz et al., 2016 and reference therein), and Asaluyeh between 17 Ma and 9 Ma (Pirouz et al., 2016 and reference therein). The present foredeep and forebulge are located in the Persian Gulf (Pirouz et al., 2016 and reference therein). The present average elevation is ~1,500 m in the Zagros orogenic belt (Figure 12).

In the Himalayan-Tibetan orogenic system, the earliest peripheral foreland basin deposits are ~60 Ma in the Sangdanlin region of southern Tibet (DeCelles et al., 2014). Subsequently, the foreland basin migrated to the Zhepure Mountain region by 50.6–52.8 Ma (Najman et al., 2010), the Lesser Himalaya region by 30–20 Ma (DeCelles e al., 2001; Najman, 2006), and the foothills of the Himalaya (Sub-Himalaya) by 21–16 Ma (Najman, 2006). The present southern boundary of the Himalayan-Tibetan orogenic system is defined by the Main Boundary Thrust and the Miocene to recent Siwalik foredeep depozone within the peripheral foreland basin system (DeCelles et al., 2014 and reference therein). Himalayan-Tibetan paleoaltimetry studies indicate abrupt uplift from ~2,000 m to ~5,500 m during early Miocene time (Figure 12, Ding et al., 2017; Garzione et al., 2000; Gébelin et al., 2013; Saylor et al., 2009).

Comparing the Zagros and Himalayan-Tibetan systems leads us to conclude that decreases in propagation rate of the paired fold-thrust belt and foreland basin system play an important role in the growth of high elevation orogenic plateaux (Figure 12). The Himalayan-Tibetan system displays an abrupt decrease in propagation rate starting between 20 and 15 Ma. Before the decrease, the development of the orogenic system was likely dominated by foreland-ward propagation, resulting in moderate regional elevations in the fold-thrust belt (<2,000 m). We interpret that the 60–20 Ma Himalayan-Tibetan orogenic belt might have looked like the modern Zagros orogenic system (Figure 12). After ~15 Ma, the fold-thrust belt and foreland-basin system of the Himalayan-Tibetan system only propagated ~100 km (Figure 12). This period also coincides with rapid surface uplift to high elevation (>5,000 m) in southern Tibet and the high Himalayas (Figure 12). One possible explanation for the decrease in propagation accompanied by rapid elevation increase is persistent subcritical taper conditions (Dahlen, 1990), which may have resulted from enhanced erosion due to increased monsoon activity or growth of an orographic barrier due flexural rebound following lithospheric delamination and/or breakoff (e.g. Clift and Webb, 2019).

7. Conclusions

Peripheral foreland basin deposits preserved adjacent to inter-continental suture zones provide direct constrains on the timing of the Arabia-Eurasia collision. The Upper Cretaceous-Miocene foreland basin system strata in interior Fars, south Iran is an ideal section for studying these processes. Field observations, petrographic data, detrital zircon U-Pb-Hf isotopes and trace element, and Cr-spinel analysis from this section lead to the following major conclusions:

1. The Paleocene Sachun Formation is composed entirely of radiolarian-rich chert and limestone that were derived from the Neyriz ophiolitic sequence. Upper Oligocene-lower Miocene Razak and Agah Jari formations dominantly comprise monocrystalline quartz, feldspar, volcanic, and metamorphic fragments that were sourced from Eurasia.
2. Coupled detrital zircon U-Pb-Hf isotopic and trace element data indicate that the 90-100 Ma, MOR-affinity detrital zircons first appeared in the Sachun Formation. These results indicate that an early peripheral foreland basin system developed in response to obduction of the Neyriz ophiolite onto the Arabian continent. In contrast to the simple detrital zircon age distributions of the Sachun Formation, the Razak and Agha Jari formations are characterized by the coexistence of continental arc-affinity Jurassic, Eocene-Oligocene detrital zircons and pre-Cambrian detrital zircon. The first appearance of Eurasia-affinity detrital zircon in the upper Oligocene-lower Miocene Razak Formation indicates that Arabia-Eurasia collision occurred before deposition of the 25.7–21.5 Ma Razak Formation, resulting in the development of a successor peripheral foreland basin system.
3. The similarity between Cr-spinel composition in the Neyriz ophiolitic rocks and Paleocene-Miocene foreland basin strata indicates that the mafic-ultramafic rocks continued to provide detritus to the foreland strata during deposition of these rocks.
4. The propagation rate of the fold-thrust and associated foreland basin has significant implications for the growth of the orogenic system.Before an abrupt decrease in propagation, the orogenic belt was dominated by horizontal growth with moderate elevation. After the decrease, the orogenic belt was dominated by rapid surface uplift with slow horizontal growth.

Data Availability Statement

All supplemental data are available in the supporting information file or https://data.mendeley.com/datasets/f2t8vm5d67/2 (https://doi.org/10.17632/f2t8vm5d67.2). Sample locations, sandstone petrology, detrital zircon U-Pb-Hf isotopic and trace element analysis, and Cr-spinel electron microprobe geochemical analysis presented in this article are available at: https://data.mendeley.com/datasets/f2t8vm5d67/2 (https://doi.org/10.17632/f2t8vm5d67.2).

Acknowledgments
This study was supported by grants from the Strategic Priority Research Program of the Chinese Academy of Sciences (XDA20070301) and the National Natural Science Foundation of China (41972239, 41941016). The authors thank Yahui Yue and Jing Xie for their assistance with analyses of detrital zircon U-Pb-Hf isotopes, trace elements, and Cr-spinel compositions. They are most grateful to Prof. Morteza Talebian for his logistical arrangement in Iran. They thank editor Laurent Jolivet and associate editor Mauricio Parra for handling the manuscript, as well as Mortaza Pirouz and two anonymous reviewers for their constructive and thoughtful reviews.

References

Afghah, M. (2016). Biostratigraphy, facies analysis of Upper Cretaceous-Lower Paleocene strata in south Zagros basin (southwestern Iran). *Journal of African Earth Sciences*, *119*, 171–184. https://doi.org/10.1016/j.jafrearsci.2016.04.002

Agard, P., Omrani, J., Jolivet, L., Whitechurch, H., Vrielynck, B., Spakman, W., et al. (2011). Zagros orogeny: A subduction-dominated process. *Geological Magazine*, *148*, 692–725. https://doi.org/10.1017/S001675681100046X

Alavi, M. (1994). Tectonics of the Zagros orogenic belt of Iran: New data and interpretations. *Tectonophysics*, *229*, 211–238. https://doi.org/10.1016/0040-1951(94)90030-2

Alavi, M. (2004). Regional stratigraphy of the Zagros fold-thrust belt of Iran and its proforeland evolution. *American Journal of Science*, *304*, 1–20. https://doi.org/10.2475/ajs.304.1.1

Alirezaei, S., & Hassanzadeh, J. (2012). Geochemistry and zircon geochronology of the Permian A-type Hasanrobat granite, Sanandaj-Sirjan belt: A new record of the Gondwana break-up in Iran. *Lithos*, *151*, 122–134. https://doi.org/10.1016/j.lithos.2011.11.015

Allen, M.B., & Armstrong, H.A. (2008). Arabia–Eurasia collision and the forcing of mid-Cenozoic global cooling. *Palaeogeography, Palaeoclimatology, Palaeoecology*, *265*, 52–58. https://doi.org/10.1016/j.palaeo.2008.04.021

Amirshahkarami, M., & Zebarjadi, E. (2018). Late Paleocene to Early Eocene larger benthic foraminifera biozones and microfacies in Estahbanate area, Southwest of Iran with Thetyan biozones correlation. *Carnonates and Evaporites*, *33*, 869–884. https://doi.org/10.1007/s13146-018-0464-8

Ao, S., Mao, Q., Khalatbari-Jafari, M., Windley, B.F., Song, D., Zhang, Z., et al. (2020). U–Pb age, Hf–O isotopes, and geochemistry of the Sardasht ophiolite in the NW Zagros orogen: Implications for the tectonic evolution of Neo-Tethys. *Geological Journal*, *56*, 1315–1329. https://doi.org/10.1002/gj.4011

Ao, S., Xiao, W., Khalatbari Jafari, M., Talebian, M., Chen, L., Wan, B., et al. (2016). U–Pb zircon ages, field geology and geochemistry of the Kermanshah ophiolite (Iran): From continental rifting at 79 Ma to oceanic core complex at ca. 36 Ma in the southern Neo-Tethys. *Gondwana Research*, *31*, 305–318. https://doi.org/10.1016/j.gr.2015.01.014

Azizi, H., Kazemi, T., & Asahara, Y. (2017). A-type granitoid in Hasansalaran complex, northwestern Iran: Evidence for extensional tectonic regime in northern Gondwana in the Late Paleozoic. *Journal of Geodynamics*, *108*, 56–72. https://doi.org/10.1016/j.jog.2017.05.003

Babaie, H.A., Babaei, A., Ghazi, M.A., & Arvin, M. (2006). Geochemical, $^{40}Ar/^{39}Ar$ age, and isotopic data for crustal rocks of the Neyriz ophiolite, Iran. *Canadian Journal of Earth Sciences*, *43*, 57–70. https://doi.org/10.1139/e05-111

Ballato, P., Uba, C.E., Landgraf, A., Strecker, M.R., Sudo, M., Stockli, D.F., et al. (2011). Arabia-Eurasia continental collision: Insights from late Tertiary foreland-basin evolution in the Alborz Mountains, northern Iran. *Geological Society of America Bulletin*, *123*, 106–131. https://doi.org/10.1130/B30091.1

Barber, D. E., Stockli, D. F., & Galster, F. (2019). The Proto-Zagros foreland basin in Lorestan, western Iran: Insights from multimineral detrital geothermochronometric and trace elemental provenance analysis. *Geochemistry, Geophysics, Geosystems*, *20*, 2657–2680. https://doi.org/10.1029/2019GC008185

Barber, D. E., Stockli, D. F., Horton, B. K., & Koshnaw, R. I. (2018). Cenozoic exhumation and foreland basin evolution of the Zagros orogen during the Arabia-Eurasia collision, western Iran. *Tectonics*, *37*, 4396–4420. https://doi.org/10.1029/2018TC005328

Be'eri-Shlevin, Y., Katzir, Y., Whitehouse, M. J., & Kleinhanns, I. C. (2009). Contribution of pre Pan-African crust to formation of the Arabian Nubian shield: New secondary ionization mass spectrometry U-Pb and O studies of zircon. *Geology*, *37*(10), 899–902. https://doi.org/10.1130/G30206A.1

Berberian, M., & King, G. C. P. (1981). Towards a paleogeography and tectonic evolution of Iran. *Canadian Journal of Earth Sciences*, *18*, 210–265. https://doi.org/10.1139/e81-019

Blichert-Toft, J. (2008). The Hf isotopic composition of zircon reference material 91500. *Chemical Geology*, *253*, 252–257. https://doi.org/10.1016/j.chemgeo.2008.05.014

Cai, F. L., Ding, L., Leary, R. J., Wang, H. Q., Xu, Q., Zhang, L. Y., & Yue, Y. H. (2012). Tectonostratigraphy and provenance of an accretionary complex within the Yarlung–Zangpo suture zone, southern Tibet: Insights into subduction-accretion processes in the Neo-Tethys. *Tectonophysics*, *574–575*, 181–192. https://doi.org/10.1016/j.tecto.2012.08.016

Chiu, H.-Y., Chung, S.-L., Zarrinkoub, M. H., Melkonyan, R., Pang, K.-N., Lee, H.-Y., et al. (2017). Zircon Hf isotopic constraints on magmatic and tectonic evolution in Iran: Implications for crustal growth in the Tethyan orogenic belt. *Journal of Asian Earth Sciences*, *145*, 652–669. https://doi.org/10.1016/j.jseaes.2017.06.011

Chiu, H.-Y., Chung, S.-L., Zarrinkoub, M. H., Mohammadi, S. S., Khatib, M. M., & Iizuka, Y. (2013). Zircon U-Pb age constraints from Iran on the magmatic evolution related to Neotethyan subduction and Zagros orogeny. *Lithos*, *162*, 70–87. https://doi.org/10.1016/j.lithos.2013.01.006

Clift, P. D., & Webb, A. A. G. (2019). A history of the Asian monsoon and its interactions with solid Earth tectonics in Cenozoic South Asia. *Geological Society, London, Special Publications*, *483*. https://doi.org/10.1144/SP483.1

Dahlen, F. A. (1990). Critical taper model of fold-and-thrust belts and accretionary wedges. *Annual Review of Earth and Planetary Sciences*, *18*, 55–99. https://doi.org/10.1146/annurev.ea.18.050190.000415

Davoudian, A. R., Genser, J., Neubauer, F., & Shabanian, N. (2016). $^{40}Ar/^{39}Ar$ mineral ages of eclogites from North Shahrekord in the Sanandaj-Sirjan Zone, Iran: Implications for the tectonic evolution of Zagros orogen. *Gondwana Research*, *37*, 216–240. https://doi.org/10.1016/j.gr.2016.05.013

DeCelles, P. G., Kapp, P., Gehrels, G. E., & Ding, L. (2014). Paleocene-Eocene foreland basin evolution in the Himalaya of southern Tibet and Nepal: Implications for the age of initial India-Asia collision. *Tectonics*, *33*(5), 824–849. https://doi.org/10.1002/2014TC003522

DeCelles, P. G., Robinson, D. M., Quade, J., Ojha, T. P., Garzione, C. N., Copeland, P., & Upreti, B. N. (2001). Stratigraphy, structure, and tectonic evolution of the Himalayan fold-thrust belt in western Nepal. *Tectonics*, *20*, 487–509. https://doi.org/10.1029/2000TC001226

Delaloye, M., & Desmons, J. (1980). Ophiolites and melange terranes in Iran: A geochronological study and its paleotectonic implications. *Tectonophysics*, *68*, 83–111. https://doi.org/10.1016/0040-1951(80)90009-8

Dick, H. J. B., & Bullen, T. (1984). Chromian spinel as a petrogenetic indicator in abyssal and alpinetype peridotites and spatially associated lavas. *Contributions to Mineralogy and Petrology*, *86*, 54–76. https://doi.org/10.1007/BF00373711

Dickinson, W., & Gehrels, G. (2009). Use of U–Pb ages of detrital zircons to infer maximum depositional ages of strata: A test against a Colorado Plateau Mesozoic database. *Earth and Planetary Science Letters*, *288*, 115–125. https://doi.org/10.1016/j.epsl.2009.09.013

Dickinson, W. R. (1985). Interpreting provenance relations from detrital modes of sandstone. In G. Zuffa (Ed.), *Provenance of arenites* (pp. 333–361). Dordrecht: Reidel Publishing Co. https://doi.org/10.1007/978-94-017-2809-6_15

Ding, L., Qasim, M., Jadoon, I. A. K., Khan, M. A., Xu, Q., Cai, F., et al. (2016). The India–Asia collision in North Pakistan: Insight from the U–Pb detrital zircon provenance of Cenozoic foreland basin. *Earth and Planetary Science Letters*, *455*, 49–61. https://doi.org/10.1016/j.epsl.2016.09.003

Ding, L., Spicer, R. A., Yang, J., Xu, Q., Cai, F., Li, S., et al. (2017). Quantifying the rise of the Himalaya Orogen and implications for the South Asian monsoon. *Geology*, *45*, 215–218. https://doi.org/10.1130/G38583.1

Fakhari, M. D., Axen, G. J., Horton, B. K., Hassan- zadeh, J., & Amini, A. (2008). Revised age of proximal deposits in the Zagros foreland basin and implications for Cenozoic evolution of the High Zagros. *Tectonophysics*, *451*, 170–185. https://doi.org/10.1016/j.tecto.2007.11.064

Falcon, N. L. (1974). Southern Iran: Zagros Mountains. *Geological Society, London, Special Publications*, *4*(1), 199–211. https://doi.org/10.1144/GSL.SP.2005.004.01.11

Garzanti, E., Vermeesch, P., Ando, S., Vezzoli, G., Valagussa, M., Allen, K., et al. (2013). Provenance and recycling of Arabian desert sand. *Earth-Science Reviews*, *120*, 1–19. https://doi.org/10.1016/j.earscirev.2013.01.005

Garzione, C. N., Quade, J., DeCelles, P. G., & English, N. B. (2000). Predicting paleoelevation of Tibet and the Himalaya from $\delta^{18}O$ vs. altitude gradients in meteoric water across the Nepal Himalaya. *Earth and Planetary Science Letters*, *183*, 215–229. https://doi.org/10.1016/S0012-821X(00)00252-1

Gébelin, A., Mulch, A., Teyssier, C., Jessup, M. J., Law, R. D., & Brunel, M. (2013). The Miocene elevation of Mount Everest. *Geology*, *41*, 799–802. https://doi.org/10.1130/G34331.1

Grimes, C. B., Wooden, J. L., Cheadle, M. J., & John, B. E. (2015). "Fingerprinting" tectono-magmatic provenance using trace elements in igneous zircon. *Contributions to Mineralogy and Petrology*, *170*, 46. https://doi.org/10.1007/s00410-015-1199-3

Habibi, T., & Ruban, D. A. (2018). Geoheritage of the Neyriz ophiolite-related radiolarite sequence (Cretaceous; southwest Iran): First report and evaluation in regional and global contexts. *Journal of African Earth Sciences*, *145*, 227–233. https://doi.org/10.1016/j.jafrearsci.2018.05.023

Hacker, B. R. (1994). Rapid emplacement of young oceanic lithosphere: Argon geochronology of the Oman ophiolite. *Science*, *265*(5178), 1563–1565. https://doi.org/10.1126/science.265.5178.1563

Hallam, A. (1976). Geology and plate tectonics interpretation of the sediments of the Mesozoic radiolarite-ophiolite complex in the Neyriz region, southern Iran. *The Geological Society of America Bulletin*, *87*, 47–52. https://doi.org/10.1130/0016-7606(1976)87<47:gaptio>2.0.co;2

Hansman, R. J., Ring, U., Thomson, S. N., Brok, B., & Stübner, K. (2017). Late Eocene uplift of the Al Hajar Mountains, Oman, supported by stratigraphy and low-temperature thermochronology. *Tectonics*, *36*, 3081–3109. https://doi.org/10.1002/2017TC0046710.1002/2017tc004672

Hassanzadeh, J., & Wernicke, B. P. (2016). The Neotethyan Sanandaj-Sirjan zone of Iran as an archetype for passive margin-arc transitions. *Tectonics*, *35*, 586–621. https://doi.org/10.1002/2015TC003926

Hatzfeld, D., & Molnar, P. (2010). Comparisons of the kinematics and deep structures of the Zagros and Himalaya and of the Iranian and Tibetan Plateaus and Geodynamic implications. *Reviews of Geophysics*, *48*, RG2005. https://doi.org/10.1029/2009RG000304

Homke, S., Vergés, J., van der Beek, P., Fernàndez, M., Saura, E., Barbero, L., et al. (2010). Insights in the exhumation history of the NW Zagros from bedrock and detrital apatite fission-track analysis: Evidence for a long-lived orogeny. *Basin Research*, *22*(5), 659–680. https://doi.org/10.1111/j.1365-2117.2009.00431.x

Honarmand, M., Li, X. H., Nabatian, G., & Neubauer, F. (2017). In-situ zircon U-Pb age and Hf-O isotopic constraints on the origin of the Hasan-Robat A-type granite from Sanandaj-Sirjan zone, Iran: Implications for reworking of Cadomian arc igneous rocks. *Mineralogy and Petrology*, *111*(5), 659–675. https://doi.org/10.1007/s00710-016-0490-y

Horton, B. K., Hassanzadeh, J., Stockli, D. F., Axen, G. J., Gillis, R. J., Guest, B., et al. (2008). Detrital zircon provenance of Neoproterozoic to Cenozoic deposits in Iran: Implications for chronostratigraphy and collisional tectonics. *Tectonophysics*, *451*, 97–122. https://doi.org/10.1016/j.tecto.2007.11.063

Hosseini, M. R., Hassanzadeh, J., Zlirezaei, S., Sun, W. D., & Li, C. Y. (2017). Age revision of the Neotethyan arc migration into the southeast Urumieh-Dokhtar belt of Iran: Geochemistry and U–Pb zircon geochronology. *Lithos*, *284–285*, 296–309. https://doi.org/10.1016/j.lithos.2017.03.012

Jackson, S. E., Pearson, N.J., Griffin, W. L., & Belousova, E. A. (2004). The application of laser ablation-inductively coupled plasma-mass spectrometry to in situ U–Pb zircon geochronology. *Chemical Geology*, *211*, 47–69. https://doi.org/10.1016/j.chemgeo.2004.06.017

James, G. A., & Wynd, J. G. (1965). Stratigraphic nomenclature of Iranian Oil Consortium agreement area. *Bulletin of the American Association of Petroleum Geologists*, *49*, 2182–2245. https://doi.org/10.1306/a663388a-16c0-11d7-8645000102c1865d

Kamenetsky, V. S., Anthony, J. C., & Sebastien, M. (2001). Factors controlling chemistry of magmatic spinel: An empirical study of associated olivine, Cr–spinel and melt inclusions from primitive rocks. *Journal of Petrology*, *42*, 655–671. https://doi.org/10.1093/petrology/42.4.655

Khadivi, S., Mouthereau, F., Barbarand, J., Adatte, T., & Lacombe, O. (2012). Constraints on palaeodrainage evolution induced by uplift and exhumation on the southern flank of the Zagros-Iranian Plateau. *Journal of the Geological Society*, *169*, 83–97. https://doi.org/10.1144/0016-76492011-031

Khadivi, S., Mouthereau, F., Larrasoana, J. C., Verges, J., Lacombe, O., Khademi, E., et al. (2010). Magnetochronology of synorogenicMiocene foreland sediments in the Fars arc of the Zagros Folded Belt (SWIran). *Basin Research*, *22*, 918–932. https://doi.org/10.1111/j.1365-2117.2009.00446.x

Koshnaw, R.I., Stockli, D. F., & Schlunegger, F. (2019). Timing of the Arabia-Eurasia continental collision: Evidence from detrital zircon U-Pb geochronology of the Red Bed Series strata of the northwest Zagros hinterland, Kurdistan region of Iraq. *Geology*, *47*, 47–50. https://doi.org/10.1130/G45499.1

Lanphere, M. A., & Pamic, J. (1983). $^{40}Ar/^{39}Ar$ ages and tectonic setting of ophiolite from the Neyriz area southeast Zagros range Iran. *Tectonophysics*, *96*, 245–256. https://doi.org/10.1016/0040-1951(83)90220-2

Li, X., Tang, G., Gong, B., Yang, Y. H., Hou, K., Hu, Z., et al. (2013). Qinghu zircon: A working reference for microbeam analysis of U-Pb age and Hf and O isotopes. *Chinese Science Bulletin*, *58*, 4647–4654. https://doi.org/10.1007/s11434-013-5932-x

Mazhari, S. A., Amini, S., Ghalamghash, J., & Bea, F. (2011). Petrogenesis of granitic unit of Naqadeh complex, Sanandaj-Sirjan Zone, NW Iran. *Arabian Journal of Geosciences*, *4*, 59–67. https://doi.org/10.1007/s12517-009-0077-6

McQuarrie, N., & van Hinsbergen, D. J. J. (2013). Retrodeforming the Arabia-Eurasia collision zone: Age of collision versus magnitude of continental subduction. *Geology*, *41*, 315–318. https://doi.org/10.1130/G33591.1

Mirzaee, M. R. (2014). Sequence microbiostratigraphy of Jahrum and Asmari Formation in Shiraz Area, Zagros, Fars, Iran. *Open Journal of Geology*, *4*, 93–107. https://doi.org/10.4236/ojg.2014.44009

Monsef, I., Monsef, R., Mata, J., Zhang, Z. Y., Pirouz, M., Rezaeian, M. m, et al. (2018). Evidence for an early-MORB to fore-arc evolution within the Zagros suture zone: Constraints from zircon U-Pb geochronology and geochemistry of the Neyriz ophiolite (South Iran). *Gondwana Research*, *62*, 287–305. https://doi.org/10.1016/j.gr.2018.03.002

Morel, M. L. A., Nebel, O., Nebel-Jacobsen, Y. J., Miller, J. S., & Vroon, P. Z. (2008). Hafnium isotope characterization of the GJ-1 zircon reference material by solution and laser-ablation MC-ICPMS. *Chemical Geology*, *255*, 231–235. https://doi.org/10.1016/j.chemgeo.2008.06.040

Morley, C. K., Kongwung, B., Julapour, A. A., Abdolghafourian, M., Hajian, M., & Waples, D. (2009). Structural development of a major late Cenozoic basin and transpressional belt in central Iran: The Central Basin in the Qom-Saveh area. *Geosphere*, *5*(4), 325–362. https://doi.org/10.1130/GES00223.1

Mouthereau, F., Lacombe, O., & Verges, J. (2012). Building the Zagros collisional orogen: Timing, strain distribution and the dynamics of Arabia/Eurasia plate convergence. *Tectonophysics*, *532–535*, 27–60. https://doi.org/10.1016/j.tecto.2012.01.022

Mouthereau, F., Tensi, J., Bellahsen, N., Lacombe, O., De Boisgrollier, T., & Kargar, S. (2007). Tertiary sequence of deformation in a thin-skinned/thick-skinned collision belt: The Zagros Folded Belt (Fars, Iran). *Tectonics*, *26*, TC5006. https://doi.org/10.1029/2007TC002098

Nadjafi, M., Mahboubi, A., Moussavi-Harami, R., & Mirzaee, M. R. (2004). Depositional History and Sequence Stratigraphy of Outcropping Tertiary Carbonates in the Jahrum and Asmari Formations, Shiraz Area (SW Iran). *Journal of Petroleum Geology*, *27*, 179–190. https://doi.org/10.1111/j.1747-5457.2004.tb00052.x

Najafi, M., Beamud, E., Ruh, J., Mouthereau, F., Tahmasbi, A., Bernaola, G., et al. (2020). Pliocene growth of the Dowlatabad syncline in Frontal Fars arc: Folding propagation across the Zagros Fold Belt, Iran. *The Geological Society of America Bulletin*, *133*. https://doi.org/10.1130/B35748.1

Najman, Y. (2006). The detrital record of orogenesis: A review of approaches and techniques used in the Himalayan sedimentary basins. *Earth-Science Reviews*, *74*, 1–72. https://doi.org/10.1016/j.earscirev.2005.04.004

Najman, Y., Appel, E., Boudagher-Fadel, M., Bown, P., Carter, A., Garzanti, E., et al. (2010). Timing of India-Asia collision: Geological biostratigraphic, and paleomagnetic constraints. *Journal of Geophysical Research*, *115*, B12416. https://doi.org/10.1029/2010JB007673

Okay, A. I., Zattin, M., & Cavazza, W. (2010). Apatite fission-track data for the Miocene Arabia-Eurasia collision. *Geology*, *38*, 35–38. https://doi.org/10.1130/G30234.1

Pirouz, M. (2018). Post-collisional deposits in the Zagros foreland basin: Implications for diachronous underthrusting. *International Journal of Earth Sciences*, *107*, 1603–1621. https://doi.org/10.1007/s00531-017-1561-y

Pirouz, M., Avouac, J.-P., Hassanzadeh, J., Kirschvink, J. L., & Bahroudi, A. (2017). Early Neogene foreland of the Zagros, implications for the initial closure of the Neo-Tethys and kinematics of crustal shortening. *Earth and Planetary Science Letters*, *477*, 168–182. https://doi.org/10.1016/j.epsl.2017.07.046

Pirouz, M., Simpson, G., Bahroudi, A., & Azhdari, A. (2011). Neogene sediments and modern depositional environments of the Zagros foreland basin system. *Geological Magazine*, *148*, 838–853. https://doi.org/10.1017/S0016756811000392

Pirouz, M., Simpson, G., Castelltort, S., Gorin, G., & Bahroudi, A. (2016). Controls on the sequence stratigraphic architecture of the Neogene Zagros foreland basin. *Geological Society of America Special Paper*, *525*, SPE525–512. https://doi.org/10.1130/2016.2525(12)

Robin, C., Gorican, S., Guillocheau, F., Razin, P., Dromart, G., & Mosa ffa, H. (2010). Mesozoic deep-water carbonate deposits from the southern Tethyan passive margin in Iran (Pichakun nappes, Neyriz area): Biostratigraphy, facies sedimentology and sequence stratigraphy. In P. Leturmy, & C. Robin (Eds.), *Tectonic and stratigraphic evolution of Zagros and Makran during the Mesozoic-Cenozoic* (pp. 179–210). Geological Society, London, Special Publications. https://doi.org/10.1144/sp330.10

Ryan, W. B. F., Carbotte, S. M., Coplan, J., O'Hara, S., Melkonian, A., Arko, R., et al. (2009). Global multi-resolution topography (GMRT) synthesis data set. *Geochemistry, Geophysics, Geosystems*, *10*, Q03014. https://doi.org/10.1029/2008GC002332

Saura, E., Garcia-Castellanos, D., Casciello, E., Parravano, V., Urruela, A., & Vergés, J. (2015). Modeling the flexural evolution of the Amiran and Mesopotamian foreland basins of NW Zagros (Iran-Iraq). *Tectonics*, *34*, 377–395. https://doi.org/10.1002/2014TC003660

Saura, E., Verges, J., Homke, S., Blanc, E., Serra-Kiel, J., Bernaola, G., et al. (2011). Basin architecture and growth folding of the NW Zagros early foreland basin during the Late Cretaceous and early Tertiary. *Journal of the Geological Society*, *168*, 235–250. https://doi.org/10.1144/0016-76492010-092

Saylor, J. E., Quade, J., Dellman, D. L., DeCelles, P. G., Kapp, P. A., & Ding, L. (2009). The late Miocene through present paleoelevation history of southwestern Tibet. *American Journal of Science*, *309*, 1–42. https://doi.org/10.2475/01.2009.01

Searle, M., & Cox, J. (1999). Tectonic setting, origin, and obduction of the Oman ophiolite. *The Geological Society of America Bulletin*, *111*, 104–122. https://doi.org/10.1130/0016-7606(1999)111<0104:tsoaoo>2.3.co;2

Shafaii Moghadam, H., Brocker, M., Griffin, W. L., Li, X. H., Chen, R. X., & O'Reilly, S. Y. (2017). Subduction, high-P metamorphism, and collision fingerprints in South Iran: Constraints from zircon U-Pb and mica Rb-Sr geochronology. *Geochemistry, Geophysics, Geosystems*, *18*, 306–332. https://doi.org/10.1002/2016GC006585

Shafaii Moghadam, H., Corfu, F., & Stern, R. J. (2013). U-Pb zircon ages of Late Cretaceous Nain-Dehshir ophiolites, central Iran. *Journal of the Geological Society*, *170*(1), 175–184. https://doi.org/10.1144/jgs2012-066

Shakerardakani, F., Li, X. H., Neubauer, F., Ling, X. X., Li, J., Monfaredi, B., & Wu, L. G. (2020). Genesis of early cretaceous leucogranites in the Central Sanandaj–Sirjan zone, Iran: Reworking of Neoproterozoic metasedimentary rocks in an active continental margin. *Lithos*, *352–353*, 105330. https://doi.org/10.1016/j.lithos.2019.105330

Sherkati, S., & Letouzey, J. (2004). Variation of structural style and basin evolution in the central Zagros (Izeh zone and Dezful Embayment), Iran. *Marine and Petroleum Geology*, *21*(5), 535–554. https://doi.org/10.1016/j.marpetgeo.2004.01.007

Sláma, J., Kosler, J., Condon, D. J., Crowely, J. L., Gerdes, A., Hanchar, J. M., et al. (2008). Plesovice zircon: A new natural reference material for U-Pb and Hf isotopic microanalysis. *Chemical Geology*, *249*(1–2), 1–35. https://doi.org/10.1016/j.chemgeo.2007.11.005

Stocklin, J. (1968). Structural history and tectonics of Iran; a review. *AAPG Bulletin*, *52*(7), 1229–1258. https://doi.org/10.1306/5d25c4a5-16c1-11d7-8645000102c1865d

Verdel, C., Wernicke, B. P., Hassanzadeh, J., & Guest, B. (2011). A Paleogene extensional arc flare-up in Iran. *Tectonics*, *30*, TC3008. https://doi.org/10.1029/2010TC002809

Vervoort, J. D. (2010). Hf analyses in zircon by LA-MC-ICPMS: Promise and pitfalls. In *Geological society of America abstract programs* (pp. 286–289). (Abstract).

Warren, C. J., Parrish, R. R., Waters, D. J., & Searle, M. P. (2005). Dating the geologic history of Oman's Semail ophiolite: Insights from U-Pb geochronology. *Contributions to Mineralogy and Petrology*, *150*, 403–422. https://doi.org/10.1007/s00410-005-0028-5

Whitechurch, H., Omrani, J., Agard, P., Humbert, F., Montigny, R., & Jolivet, L. (2013). Evidence for Paleocene-Eocene evolution of the foot of the Eurasian margin (Kermanshah ophiolite, SW Iran) from bacK-Arc to arc: Implications for regional geodynamics and obduction. *Lithos*, *182–183*, 11–32. https://doi.org/10.1016/j.lithos.2013.07.017

Yin, A., & Harrison, T. M. (2000). Geologic evolution of the Himalayan-Tibetan orogen. *Annual Review of Earth and Planetary Sciences*, *28*, 211–280. https://doi.org/10.1146/annurev.earth.28.1.211

Zadeh, P. G., Adabi, M. H., Ghassemi, M. R., Sadeghi, A., & Eshraghi, S. A. (2020). Mélange development in the Neyriz region of Zagros Orogen, Iran: Record of convergence and collision in the Neotethyan Realm. *Basin Research*, *32*, 1626–1652. https://doi.org/10.1111/bre.12445

Zhang, Z., Xiao, W., Ji, W., Majidifard, M. R., Rezaeian, M., Talebian, M., et al. (2018). Geochemistry, zircon U-Pb and Hf isotope for granitoids, NW Sanandaj-Sirjan zone, Iran: Implications for Mesozoic-Cenozoic episodic magmatism during Neo-Tethyan lithospheric subduction. *Gondwana Research*, *62*, 227–245. https://doi.org/10.1016/j.gr.2018.04.002

Zhang, Z., Xiao, W., Majidifard, M. R., Zhu, R., Wan, B., Ao, S., et al. (2017). Detrital zircon provenance analysis in the Zagros Orogen, SW Iran: Implications for the amalgamation history of the Neo-Tethys. *International Journal of Earth Sciences*, *106*, 1223–1238. https://doi.org/10.1007/s00531-016-1314-3

Reference From the Supporting Information

Grimes, C. B., John, B. E., Kelemen, P. B., Mazdab, F. K., Wooden, J. L., Cheadle, M. J., et al. (2007). Trace element chemistry of zircons from oceanic crust: A method for distinguishing detrital zircon provenance. *Geology*, *35*, 643–646. https://doi.org/10.1130/g23603a.1. https://doi.org/10.1130/G23603A.1